nature chemical biology

Article

https://doi.org/10.1038/s41589-026-02168-3

Genetic recording and in situ readout of single-cell signaling memory

Received: 11 February 2025

Accepted: 10 February 2026

Published online: 11 March 2026

Check for updates

Kai Hao[1], Yunzheng Liu[2], Mykel Barrett[1], Zainalabedin Samadi[1], Amirhossein Zarezadeh[1], Yuka McGrath[1], Magdalena Zernicka-Goetz[2,3] & Amjad Askary[1]

Intensity and duration of biological signals encode a few pathways to direct diverse cellular behaviors, yet quantifying these features in single cells remains difficult. To address this challenge, we developed INSCRIBE, which uses a CRISPR base editor to mutate genomic targets at rates proportional to signaling activity. Edits are recovered at the endpoint through a new ratiometric readout strategy from images of two fluorescence channels. We engineered human cells to record WNT and BMP activity. Following defined exogenous stimulations, INSCRIBE accurately recovered signal intensity in dose–response experiments and exposure duration in time-course experiments. Applying INSCRIBE revealed a persistent memory in the BMP pathway, where progeny of high-responding cells remained more sensitive to subsequent BMP stimulation for up to 3 weeks. Together, our results establish a scalable platform for genetic recording and in situ readout of signaling activity in single cells, advancing quantitative analysis of cell–cell communication during development and disease.

In multicellular organisms, the behavior and fate of cells are orchestrated by signaling pathways. Cells interpret the intensity and duration of signals to produce the appropriate response. During development, signaling gradients provide spatial and temporal cues that guide cell fate decisions[1–3]. During immune responses, the amplitude and duration of T cell antigen receptor signaling determine whether a T cell activates, proliferates and differentiates or becomes tolerant[4]. Similarly, neoplastic cell division and cancer metastasis often involve aberrant signaling levels. WNT (wingless and integrase-1) signaling is frequently dysregulated in different types of cancer, and pathway activity serves as a prognostic indicator of patient outcome[5]. In all these contexts, explaining or predicting cellular behavior hinges on accurately measuring signaling pathway activity in individual cells over time.

The importance of cell signaling has spurred development of several strategies for capturing the molecular history of cells[1,6]. Time-lapse microscopy offers a direct window into signaling dynamics with exceptional temporal resolution. However, it is limited to optically accessible samples and relatively short time scales. Despite substantial progress in microscopy techniques, it remains difficult to reliably track large numbers of cells in complex in vivo environments over extended time periods.

Genetic engineering provides an alternative to direct observation. Using site-specific recombination, cells can be permanently labeled following pathway activation. This powerful technique has enabled numerous groundbreaking discoveries[7]. However, in its simple form (for example, Cre–Lox recombination with a single *loxP*-flanked cassette), it only produces a binary outcome, precluding quantitative association of signaling levels and cellular phenotypes.

Advances in molecular recording allow cells to write aspects of their signaling history into their genome as targeted mutations that can be detected at a later time (Fig. 1a). This approach is enabled by the multitude of genome editing methods, including recombinases[8–10], CRISPR–Cas9 (refs. 11–15), CRISPR intergrases[16–18], base editors[19–21] and prime editors[22–24]. The pattern and frequency of mutations can be used to reconstruct lineage and molecular history of cells[25–28]. Recording longitudinal information in the genome enables high-throughput

[1]Department of Molecular, Cell and Developmental Biology, University of California, Los Angeles, Los Angeles, CA, USA. [2]Biology and Biological Engineering, California Institute of Technology, Pasadena, CA, USA. [3]Department of Physiology, Development and Neuroscience, Downing Site, University of Cambridge, Cambridge, UK. e-mail: amjada@ucla.edu

https://doi.org/10.1038/s41589-026-02168-3

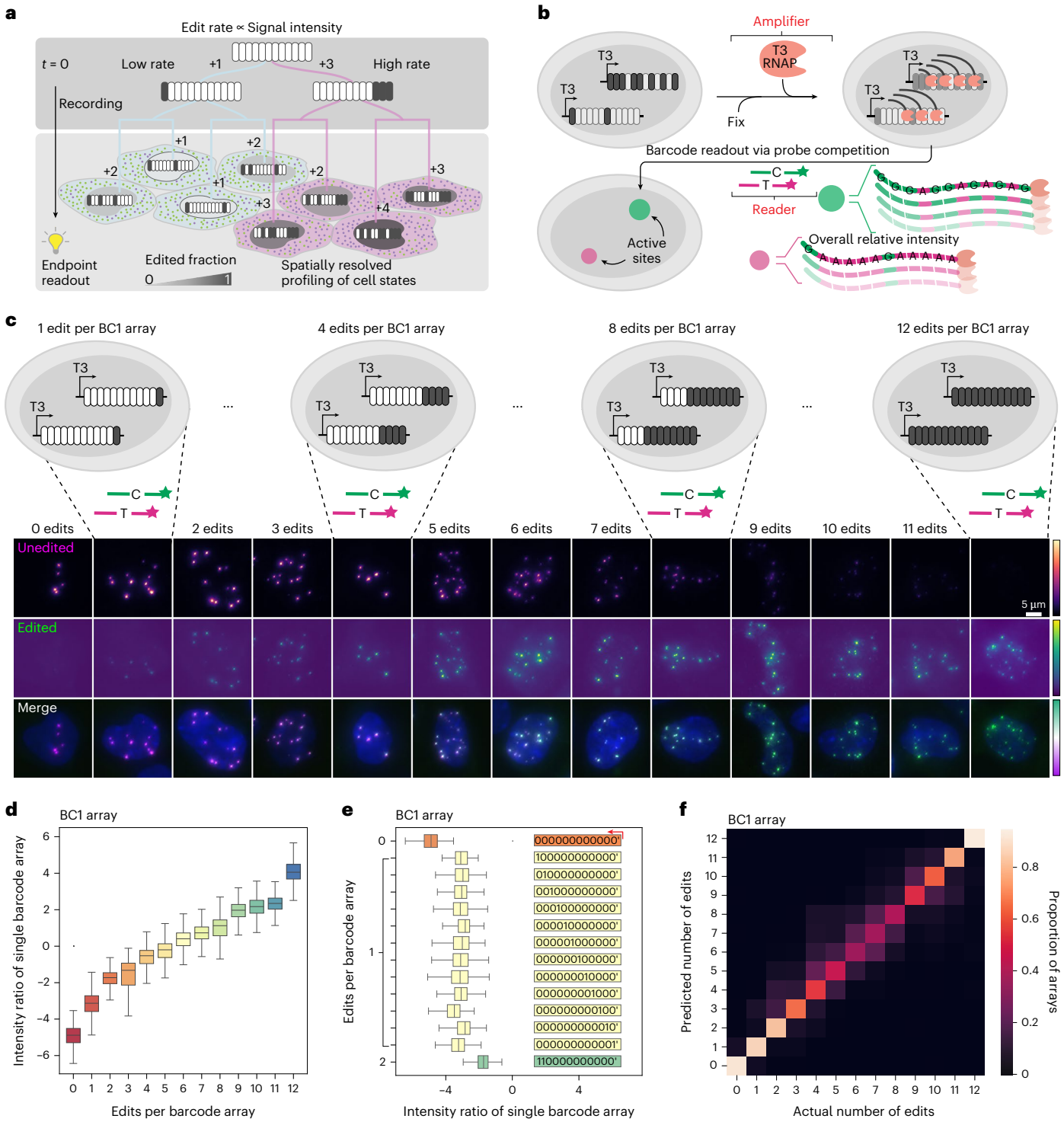

Fig. 1 | Molecular recording with in situ ratiometric barcode readout. **a**, Schematic for recording signaling activity by accumulated barcode edits through cell lineages. Each barcode is a genomic site that can be edited to provide two possible states (white or gray). Barcode edits can be read out together with spatial information and gene expression at the endpoint. Nuclei are shaded in varying grayscales, representing the fraction of edited barcodes. **b**, Ratiometric barcode readout workflow. Barcode arrays are transcribed in situ. Accumulation of transcripts in the active site amplifies the signal. Barcode transcripts are hybridized with an equimolar mixture of two fluorescent probes that differ by a single nucleotide, corresponding to the edited (C) and unedited (T) states. Their competitive binding yields relative intensities reflecting the fraction of edited barcodes; RNAP, RNA polymerase. **c**, Representative images of BC1 array cells with known edit states. Each column shows one edit level, with unedited and edited probes shown in magenta and green. Channels were contrast adjusted using fixed display ranges (unedited: 200–8,000; edited: 400–8,000), as indicated by the color scales. The merged image color bar schematically represents the edited/unedited intensity ratio. **d**,**e**, Box plot analysis of $\log_2$-scaled edited/unedited intensity ratios for BC1 arrays. Ratios increase with edit number (**d**). Arrays with one edit show similar ratios regardless of edit position, falling between those of arrays with zero or two edits. '1' denotes an edited barcode, '0' denotes an unedited barcode, and the red arrow marks the direction of T3 transcription (**e**). Boxes represent the interquartile range (IQR), center lines denote medians, and whiskers extend to 1.5× IQR (outliers omitted). **f**, BC1 array edit number inferred from two-color fluorescence images using a CNN classifier. A confusion matrix compares the true against the predicted edit numbers, with frequency normalized for each row summing to one.

snapshot methods, such as single-cell sequencing and spatial genomics, to capture both history and endpoint cell states[29], circumventing the need for real-time observation.

An ideal signal recording system should provide accurate single-cell measurements, preserve spatial context, be compatible with gene expression profiling, support multiplexed recording and remain practical without specialized equipment. Sequencing-based approaches are promising but disrupt spatial organization, which is often essential for tissue biology, and have limited accuracy at the single-cell level. Existing imaging-based methods preserve spatial information, can decode many targets per cell[21] and are compatible with gene expression profiling[9]. However, the many cycles of hybridization and imaging needed to retrieve recorded information are technically challenging and time consuming, limiting the sample area that can be analyzed and curbing broader adoption.

Here, we introduce an approach for detecting the number of edits in DNA barcode arrays based on the fluorescence intensity of only two probes. This 'ratiometric barcode readout' bypasses extensive sequential hybridization and imaging processes, thereby solving the main hurdle for widespread application of imaging-based molecular recording. Using ratiometric barcode readout, we developed a scalable method for spatially resolved quantitative reconstruction of signaling activity at the single-cell level, called in situ single-cell recording of signal intensity as barcode edits (INSCRIBE). INSCRIBE uses a CRISPR A-to-G base editor (ABE) to mutate specific sites within barcode arrays that are distributed across multiple genomic loci. As testbeds, we use two deeply conserved morphogen pathways, WNT and bone morphogenetic protein (BMP), which pattern tissues across metazoans. In their canonical forms, WNT stabilizes β-catenin to drive T cell factor/lymphoid enhancer factor (TCF/LEF)-dependent transcription[30], whereas BMP signals through receptor-mediated phosphorylation of small mother against decapentaplegic (SMAD) to regulate gene expression[31]. We generated human embryonic kidney (HEK293) cell lines in which the frequency of barcode edits is proportional to activity of WNT or BMP signaling pathways. Using exogenous stimulation with CHIR-99021 (CHIR) for WNT and BMP2 for the BMP pathway, we show that either the amplitude or duration of signaling in these cell lines can be recovered from endpoint measurements. We also implemented INSCRIBE in mouse embryonic stem (mES) cells and demonstrated that orthogonal barcode arrays can be read out sequentially.

Using INSCRIBE, we analyzed single-cell variability in response to WNT and BMP stimulation. Comparing the magnitude of responses between two sequential stimulations revealed persistent memory in the BMP pathway, which can last up to 18 days. This demonstrates the utility of INSCRIBE in providing novel biological insight and addressing otherwise intractable questions.

Results

Ratiometric readout efficiently recovers barcode array states

Molecular recording involves engineering cells to accumulate mutations within predefined genomic targets, referred to here as 'barcode arrays'. If the mutation rate is proportional to the activity of a signaling pathway, the fraction of edited barcodes reflects the cumulative pathway activity in the lineage of each cell (Fig. 1a). We previously developed a method for sensitive in situ readout of DNA barcodes[32], in which a phage RNA polymerase transcribes the barcode arrays in situ and the resulting transcripts are visualized as bright spots by fluorescence in situ hybridization (FISH). Hybridization with competing probes enables accurate in situ identification of single-nucleotide edits, but reading out each barcode individually would require two fluorescence channels per barcode and many hybridization cycles. We reasoned that signaling activity could be inferred much more efficiently if all barcodes in an array are probed with the same pair of probes targeting the edited and unedited states (Fig. 1b). This 'ratiometric barcode readout' approach detects the fraction of edited barcodes in an array, instead of the state of each individual barcode, trading off acquiring unnecessary information for simplicity and scalability.

We assessed the feasibility of ratiometric barcode readout using HEK293 cell lines containing synthetic barcode arrays with known states (Methods). Each array comprised 12 barcodes, placed downstream of a T3 promoter, with a designated single nucleotide varied from A to G within each barcode to mimic the unedited or edited state (Fig. 1c and Extended Data Fig. 1a). We designed two independent barcode arrays, which shared overall architecture but with distinct protospacer sequences and PAM contexts, henceforth referred to as BC1 (Fig. 1c–f) and BC2 (Extended Data Fig. 1).

After in situ transcription by T3 RNA polymerase[32], we hybridized two fluorescently labeled probes, complementary to the edited and unedited states of the target sites. The resulting images revealed a trend: as the number of edits increased from 0 to 12, fluorescence intensity in the edited channel rose, whereas intensity in the unedited channel diminished (Fig. 1c and Extended Data Fig. 1a). This effect was quantified by calculating the ratio of fluorescence intensity in the edited channel versus the unedited channel (Fig. 1d and Extended Data Fig. 1b). Comparing barcode arrays with identical numbers of edits but different configurations showed that intensity ratio is a function of the number of edits, not their position within the array (Fig. 1e and Extended Data Fig. 1c).

Knowing the true state of each barcode array allows us to train a classifier to predict the number of edits from the microscopy image of an array. We trained a convolutional neural network (CNN) for this task, using images of 23,743 BC1 and 15,855 BC2 spots, corresponding to barcode arrays with 0 to 12 edits (Fig. 1f and Extended Data Fig. 1d). The trained classifier inferred the number of edits in barcode arrays with a macroaveraged F1 score of 0.6 for BC1 and 0.69 for BC2. Accuracy was greater for arrays with low (0 to 3) or high (10 to 12) edit counts, while most inaccurate predictions occurred for intermediate edit counts. Overall, 91.5% of BC1 arrays and 97.7% of BC2 arrays had predicted edit counts within two edits of their actual counts. This confirms that ratiometric barcode readout can infer barcode array edit levels from two-channel images and provides an automated classification tool for this purpose.

INSCRIBE enables analog recording of signaling amplitude

To demonstrate genetic recording of signaling activity with single-cell imaging-based readout, we established monoclonal HEK293 cell lines harboring three components: an inducible ABE, a signal-responsive guide RNA (gRNA) and barcode arrays compatible with ratiometric readout (Fig. 2a,b). Each array contained 12 identical target sites for a single gRNA, downstream of a T3 promoter (Fig. 2a). Each target site included a single A nucleotide within the ABE editing window, overlapping with the FISH probe sequence (Fig. 2b). ABE expression in INSCRIBE cell lines was controlled by doxycycline (Dox) using the TetOn 3G system and further regulated by an ecDHFR degron stabilized with trimethoprim (TMP) to minimize basal editing (Fig. 2c). Edit rate was coupled to BMP or WNT pathway activity using *cis*-regulatory elements (CREs) containing multimerized binding sites for BMP SMADs[33] and TCF/LEF[34], which drive production of a chimeric transcript encoding both H2B–cyan fluorescent protein (CFP) and a barcode-specific gRNA (Fig. 2a). The gRNA is released by hammerhead and hepatitis delta virus ribozymes. To test the performance of different barcode arrays, BMP recorder lines were generated with BC1 or BC2, whereas WNT recorder lines were made with BC1.

Constructs were stably integrated in HEK293 cells with three rounds of PiggyBac transposition (Methods). We then recovered and analyzed multiple monoclonal cell lines containing all INSCRIBE components. BMP signaling was induced with 64 ng ml^{-1} BMP2, and the WNT pathway was stimulated with 3 μM CHIR, a small-molecule GSK3

https://doi.org/10.1038/s41589-026-02168-3

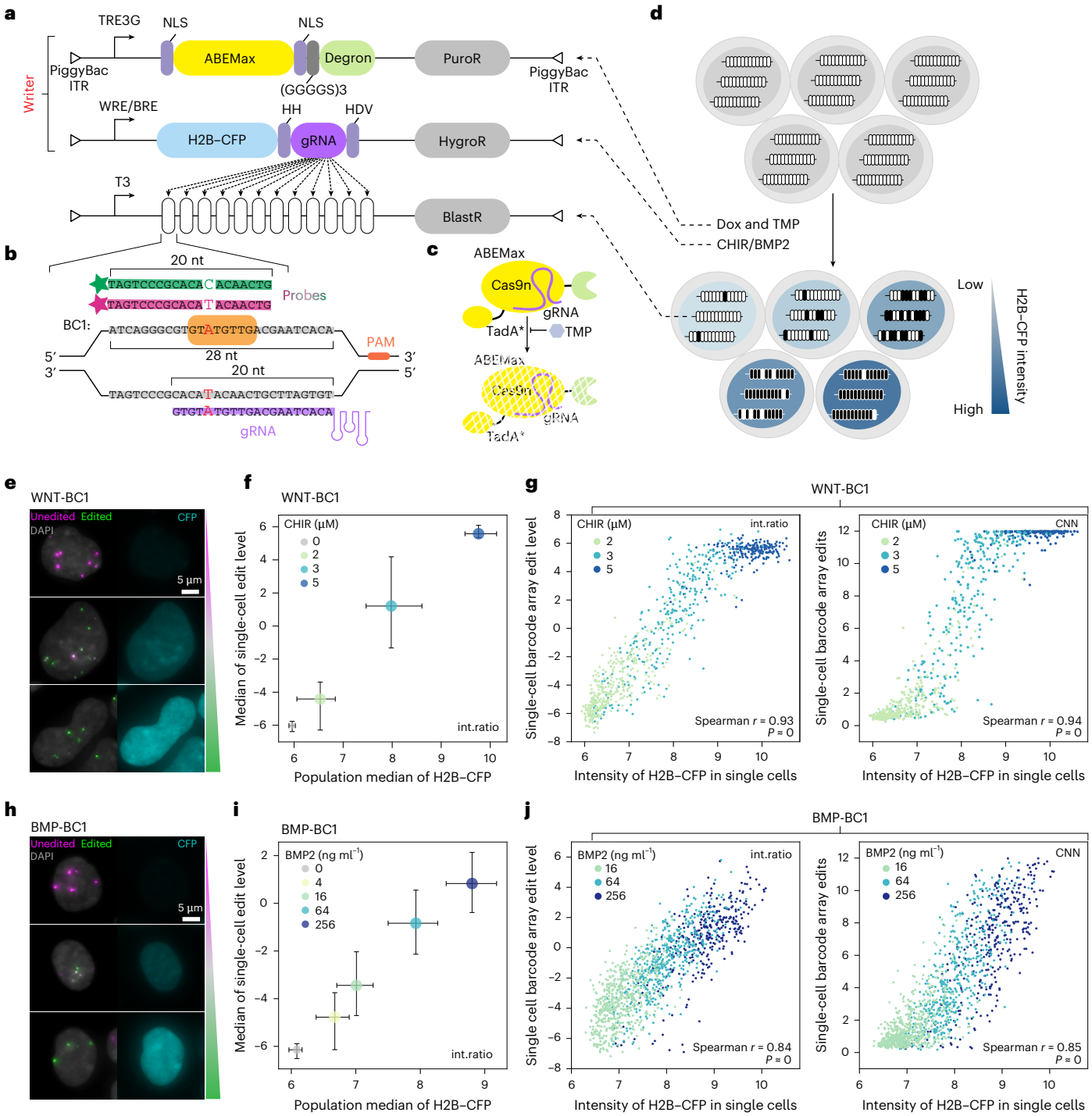

Fig. 2 | Recording WNT and BMP pathway activity in a dose-dependent manner. a, Design of INSCRIBE cell lines. Each cell contains Dox-inducible ABE, signal-responsive gRNA and H2B–CFP and barcode arrays compatible with ratiometric readout. All components are stably integrated using PiggyBac transposase; HDV, hepatitis delta virus; HH, hammerhead; ITR, inverted terminal repeat; NLS, nuclear localization signal; WRE, WNT-responsive element; BRE, BMP-responsive element; PuroR, puromycin resistance; HygroR, hygromycin resistance; BlastR, blasticidin resistance. **b**, Design of a single barcode in the BC1 array with its corresponding gRNA target site and the ratiometric probe binding site. The editing window of ABE is shaded in orange; nt, nucleotide. **c**, ABE expression is further controlled through stabilization of the ecDHFR degron by TMP. **d**, Signal-dependent gRNA expression drives barcode editing and induces H2B–CFP, which serves as a proxy for signaling activity in short-term recordings. **e**,**h**, Representative single-cell images showing the editing levels and corresponding H2B–CFP intensities for WNT-BC1 (**e**) and BMP-BC1 (**h**). Three cells are shown with ascending response levels from top to bottom. The merged image color bar schematically represents the edited/unedited intensity ratio. **f**,**i**, Scatter plots display the median single-cell edit levels versus H2B–CFP intensities for WNT-BC1 (**f**) and BMP-BC1 (**i**). Edit level is calculated as the average intensity ratios (int.ratio) across all barcode arrays in each cell. The varying levels of signal inducer are indicated by color. Bars represent the IQR. **g**,**j**, Correlation of single-cell edit levels with H2B–CFP intensities for WNT-BC1 (**g**) and BMP-BC1 (**j**). Each point represents a single cell, colored by inducer level. Edit level in each cell is calculated either as the average of intensity ratios (left) or as the average of CNN classifier-predicted edits (right) across all its barcode arrays. Spearman correlation coefficients across the inducer dosages and associated two-sided *P* values are shown for each plot. All recordings were performed over 3 days with 10 µM TMP, using 2,500 ng ml^{-1} Dox for WNT recordings (**e**–**g**) and 500 ng ml^{-1} Dox for BMP recordings (**h**–**j**).

inhibitor. Culture medium also contained 100 ng ml^{-1} Dox and 10 μM TMP. Different clones showed variability in baseline activity and sensitivity to stimulation (Extended Data Fig. 2a–c).

To assess whether INSCRIBE could record BMP and WNT signaling activity, we examined three WNT-BC1 clones, three BMP-BC1 clones and two BMP-BC2 clones, exposing each to varying concentrations of CHIR or BMP2, respectively. After stimulating the cells for 3 days, we performed ratiometric barcode readout and imaged cells in the two probe channels along with DAPI for nuclei and CFP for pathway reporter activity. The reporter for each pathway drives the expression of a chimeric transcript that cleaves into mRNA encoding H2B–CFP and barcode targeting gRNA. Because H2B–CFP protein is relatively stable and diluted primarily by cell division (every 24 to 48 h), its accumulation over the 3-day recording provides a reliable proxy for reporter activity in each cell (Fig. 2d).

In the resulting images, we simultaneously recovered barcode probe intensities for all integrations and the corresponding H2B–CFP intensity from the same cell (Fig. 2e,h and Extended Data Fig. 3a). We quantified the editing level of each cell either as the average intensity ratio or the average CNN classifier-predicted edits for all its arrays (Methods). For both the BMP and WNT pathways, the edit level increased with inducer concentration and correlated with CFP intensity at both population (Fig. 2f,i and Extended Data Fig. 3b,e) and single-cell levels (Fig. 2g,j and Extended Data Fig. 3c,f), demonstrating the ability of INSCRIBE to recover past signaling activity in individual cells. Multiple independent clones for each INSCRIBE configuration showed consistent correlation between edit level and CFP expression, confirming the reproducibility and robustness of the recording system. Across these clones, the genomic copy number of TetOn-ABE and CRE-H2B–CFP-gRNA ranged narrowly from 1 to 3, whereas barcode array copy number showed greater variability, ranging from 2 to 7 (Extended Data Fig. 2d). For all subsequent experiments, we focused on one clone for each pathway–barcode array combination with the strongest correlation between single-cell edit level and the corresponding CFP intensity across all inducer dosages, referred to as WNT-BC1, BMP-BC1 and BMP-BC2.

We observed different dynamics for BC1 and BC2 following BMP2 stimulation. BMP-BC1 cells exhibited lower edit levels than BMP-BC2 cells exposed to the same BMP2 concentration (Extended Data Fig. 3d). Accordingly, higher BMP2 concentrations (16, 64 and 256 ng ml^{-1}) led to distinct edit levels in BMP-BC1 cells (Fig. 2j), whereas BMP-BC2 cells had distinguishable edit levels for lower BMP2 concentrations (4, 16 and 64 ng ml^{-1}) and saturated at 256 ng ml^{-1} (Extended Data Fig. 3b,c). While both arrays encode single-adenine editable sites at equivalent positions within their respective protospacers, differences in local nucleotide composition, GC content and sequence-dependent ABE–DNA interactions result in array-specific base editing kinetics. Therefore, we expect that distinct barcode arrays provide different dynamic ranges, suitable for recording signals with different amplitudes.

We also asked whether the dynamic range of INSCRIBE can be tuned by regulating ABE. Varying Dox levels from 100 to 2,500 ng ml^{-1} had little effect on edit levels under any tested conditions (Extended Data Fig. 4). At 20 ng ml^{-1}, ABE induction was insufficient to record BMP pathway activity, while there were detectable edit levels in response to 5 μM CHIR. Therefore, regulation of ABE expression is effectively binary, with edit levels being a function of signaling activity once ABE expression exceeds a threshold.

Further, to contrast signal recording with snapshot measurements of downstream gene expression, we performed multiplexed single-molecule FISH (smFISH) in combination with ratiometric barcode readout. BMP-BC2 cells were stimulated with BMP2 (256 ng ml^{-1}) for 1 day, after which we imaged CFP levels, quantified transcripts encoding ID1, ID3, ID4 and SMAD6 in the same cells and performed ratiometric barcode readout (Extended Data Fig. 5a). As expected, all four downstream genes were substantially upregulated following stimulation (Extended Data Fig. 5b). The strong correlation of single-cell *ID3* mRNA counts between the first and third hybridization rounds confirmed the robustness of the multiplexed smFISH protocol (Extended Data Fig. 5c). Although the target genes were well correlated with each other, their correlation with either CFP or edit levels was modest, although statistically significant (Extended Data Fig. 5d). These results indicate that downstream gene expression provides only transient snapshots of pathway activation, in contrast to the cumulative signaling activity captured by INSCRIBE.

Together, our results show that INSCRIBE is an analog recording system capable of recovering signaling amplitude over a fixed time window from single cells. The sensitivity of INSCRIBE can be adjusted using different gRNAs. Recording works over a wide range of ABE levels, facilitating implementation of the system in other cell lines or in vivo models.

INSCRIBE enables sequential readout of barcode arrays

A key advantage of CRISPR-based genome editing tools is their capacity for multiplexing. In the INSCRIBE system, recording two signals simultaneously requires assigning each signal a distinct gRNA targeting an orthogonal barcode array. Sequential FISH has been demonstrated as a scalable strategy for detecting many targets in the same sample[35,36]. To test whether ratiometric barcode readout can be performed sequentially and to assess the adaptability of INSCRIBE in other cell types, we engineered mES cells with two independent barcode arrays (BC1 and BC2). The cells also contained an inducible ABE and a WNT-responsive gRNA targeting BC1 (Fig. 3a). If the two barcode arrays are orthogonal, edits should appear only in BC1 following WNT stimulation, and probes designed for each array should not cross-hybridize. We first recovered and characterized multiple monoclonal mES cell lines harboring the complete WNT-BC1 INSCRIBE components, using 3 μM CHIR to activate WNT signaling (Extended Data Fig. 6a). Analysis of two clones demonstrated correlated editing levels and CFP expression at both the population and single-cell scales, confirming that WNT amplitude can be recorded in mES cells (Extended Data Fig. 6b,c). Both BC1 and BC2 arrays in the two selected mES cell WNT-BC1 lines were integrated at four to five copies per cell (Fig. 3b).

We then developed a sequential ratiometric barcode readout protocol to interrogate BC1 and BC2 arrays at the single-cell level (Methods), demonstrated by iterative hybridization and probe stripping for BC1 and BC2 arrays, followed by a rehybridization of BC1 probes (Fig. 3c). Because BC1 and BC2 arrays were integrated as independent constructs, the absence of spot colocalization indicates that probes for one array do not cross-hybridize with the other (Fig. 3c). The fluorescence intensity distributions of single barcode arrays from edited and unedited channels indicated efficient probe stripping and the unedited status of BC2 arrays (Fig. 3d). We also observed a decline in the fluorescence intensity of both edited and unedited channels of BC1 between the first and third round of readout (Fig. 3d). Importantly, because the reduction was comparable in both channels, the inferred edit levels remained unaffected, as evidenced by the strong correlation of single-cell edit levels between the two BC1 hybridizations, validating the robustness of multiround ratiometric barcode readout (Fig. 3e, green). In addition, lack of correlation between single-cell edit levels of BC1 and BC2 arrays confirms orthogonal editing (Fig. 3e, purple). Together, these results show that BC1 and BC2 arrays can be edited and read out independently, establishing their suitability for multiplexed recording.

INSCRIBE can record duration of signaling activity

In addition to intensity, duration of signaling activity is crucial in regulating cellular behavior[37]. Fluorescent reporters are diluted over time by protein degradation and cell division, making signaling duration difficult to infer from endpoint measurements. By contrast, barcode edits are irreversible and heritable, enabling stable recording

https://doi.org/10.1038/s41589-026-02168-3

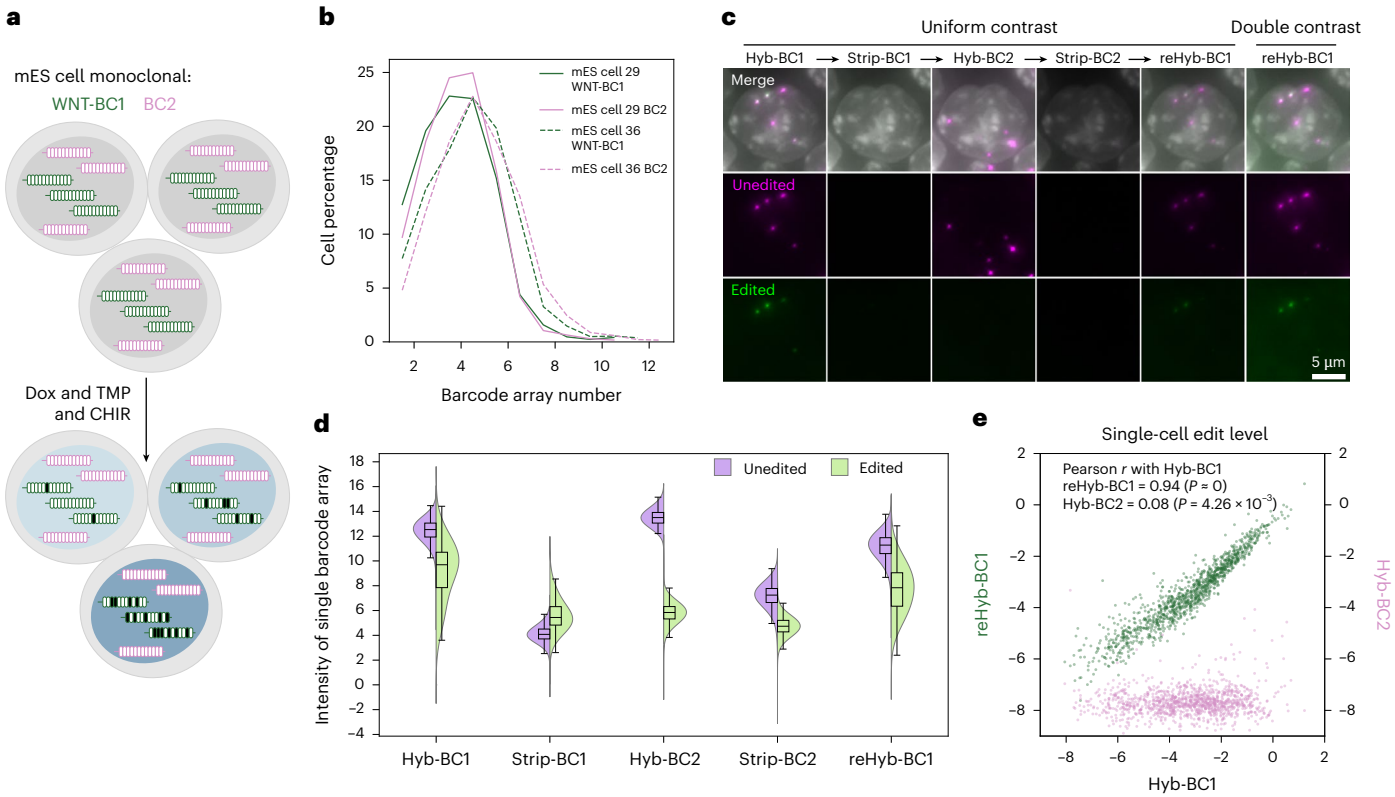

Fig. 3 | Sequential ratiometric readout of orthogonal barcode arrays in mES cells. a, Design of INSCRIBE mES cell lines with orthogonal barcode arrays. **b**, Distribution of the number of BC1 and BC2 arrays detected in individual cells for each INSCRIBE mES cell line. Even though each cell line is a monoclonal population, some variability can arise in the number of detected arrays due to efficiency of in situ transcription and imperfect segmentation. **c**, Representative images demonstrate the performance of sequential ratiometric readout for two barcode arrays. The last panel, corresponding to rehybridization of BC1, is displayed with higher contrast to emphasize that despite some decline in the absolute signal intensity over three rounds, the relative signal intensity of the two channels remains consistent; Hyb, hybridization; reHyb, rehybridization. **d**, Split violin plots showing the fluorescence intensity distributions of single barcode arrays in the unedited and edited channels, measured across multiple rounds of ratiometric readout. The overlaid boxes indicate the IQR, with center lines marking the median and whiskers extending to 1.5× IQR. Outliers are omitted for clarity. **e**, Scatter plot showing the correlation of single-cell edit levels between the first and second BC1 array hybridizations (left *y* axis, green), as well as between BC1 and BC2 arrays (right *y* axis, purple). Edit level in each cell is calculated as the average of intensity ratios across all its barcode arrays. Pearson correlation coefficients and associated two-sided *P* values are shown. All recording experiments were performed for 3 days with 500 ng ml^{-1} Dox and 10 µM TMP supplement. WNT signaling was activated by 3 µM CHIR.

of signaling history. To test whether INSCRIBE can recover signaling duration, we cultured cells under editing conditions (500 ng ml^{-1} Dox and 10 µM TMP) combined with 64 ng ml^{-1} BMP2 or 3 µM CHIR for varying durations (Fig. 4a). We estimated the average edit level in each cell from the endpoint images (Fig. 4b) based on either intensity ratio or CNN-predicted edit number per barcode array (Methods). As anticipated, barcode edits accumulated progressively over time in all cases (Fig. 4c,d). BMP-BC1 and WNT-BC1 cells showed nearly monotonic increase over 7 days, whereas BMP-BC2 cells exhibited a rapid increase in edits within the first 3 days and approached saturation by day 4, consistent with the faster edit rate of the BC2 array (Extended Data Fig. 3d). Together, our results demonstrate that INSCRIBE can record either the amplitude of a signal over a defined time period (Figs. 2 and 3) or the duration of a signal of known intensity (Fig. 4), all in a format that is image readable and can be recovered from single cells.

INSCRIBE barcode arrays are stable and efficiently used

Because our barcode arrays contain 12 tandem repeats of identical gRNA target sites, it is important to verify their long-term genomic stability. Collapse of barcode sequences, leading to loss of memory, has been observed in other molecular recording systems[38]. INSCRIBE uses base editing, which avoids double-stranded DNA breaks[39], and is therefore expected to be less prone to collapse during editing. To assess the stability and editing patterns of barcode arrays, we used long-read amplicon sequencing. Further, we combined amplicon sequencing with imaging to validate ratiometric readout against an independent method (Fig. 5a).

We amplified barcode arrays from genomic DNA from WNT-BC1 cells and BC2-only cells maintained in culture without editing for over 1 year, WNT-BC1 cells recorded for 3 days and BC2-only cells edited for 3 days after transfection. As additional controls, we included BC1 and BC2 arrays with defined edit states amplified from reference plasmids (Extended Data Fig. 7a). For all samples, amplicon sequencing revealed identical distribution of array lengths centered at the expected length of 416 base pairs (bp), confirming the stability of INSCRIBE barcode arrays (Fig. 5b and Extended Data Fig. 7b).

Sequencing results were also consistent with in situ measurement of barcode edits by ratiometric readout. The proportion of barcode arrays containing at least one edit was comparable between the two measurement modalities (paired *t*-test $P = 0.469$). Both methods measured approximately 50% edited arrays in WNT-BC1 cells grown in editing conditions for 3 days and close to 5% for the unstimulated controls (Fig. 5c). Further, within the edited barcode arrays of WNT-BC1 cells after 3 days of recording, a χ^2 test comparing the distributions of edits number estimated by in situ readout or sequencing yielded a *P* value of 0.28, indicating no statistically significant difference between the two methods (Fig. 5d). Together with our analysis of synthetic barcode arrays with known ground truth (Fig. 1), this provides further

https://doi.org/10.1038/s41589-026-02168-3

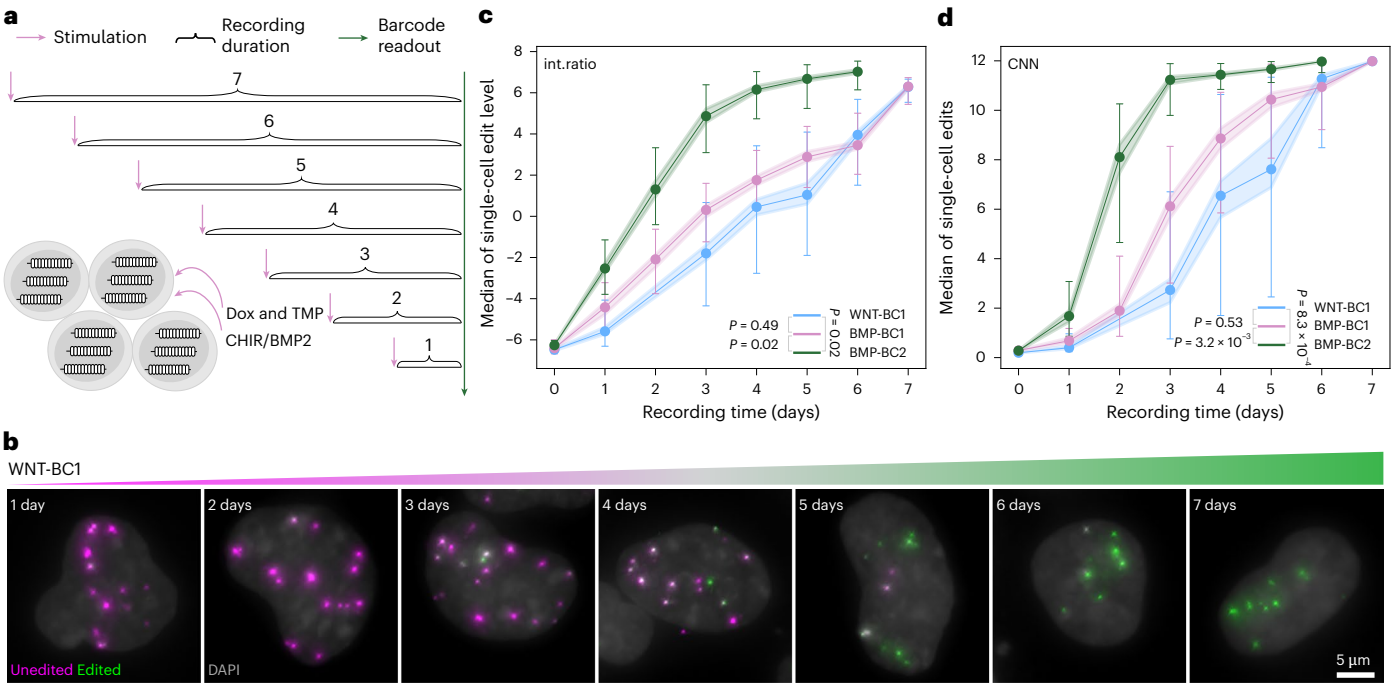

Fig. 4 | Recording duration of WNT and BMP signaling in INSCRIBE cells. **a**, Schematic of the experimental workflow for time-dependent recording of signaling activity. ABE expression was induced by 500 ng ml^{-1} Dox and 10 µM TMP. The WNT and BMP pathways were activated by the addition of 3 µM CHIR and 64 ng ml^{-1} BMP2, respectively. Cells were cultured under recording conditions for varying amounts of time and processed for ratiometric barcode readout together. **b**, Representative images show the editing level of single cells across different recording durations. The color bar for merged images is shown as a schematic of relative intensity (edited/unedited). **c**,**d**, Population median of single-cell edit levels plotted against recording time for each cell line, indicated by color coding. Edit level in each cell is calculated either as the average of intensity ratios (**c**) or as the average of CNN classifier-predicted edits (**d**) across all its barcode arrays. Bars represent the IQR, and shaded areas show the 95% confidence interval for the medians. Two-sided *F*-tests were performed on the population median of single-cell edit levels over time after fitting the linear-to-plateau model, with false discovery rate (FDR)-adjusted *P* values indicated on the plots.

assurance that ratiometric readout accurately recovers the fraction of edited sites in the arrays.

Estimating the overall signaling activity is most efficient if all target sites within an array have the same probability of being edited. If certain sites are preferentially edited, this bias should be considered when integrating the results across all barcodes. Because INSCRIBE barcodes have identical sequences and are targeted by the same gRNA, we expect them to have similar edit rates. To test this, we first confirmed that long-read amplicon sequencing accurately resolves single-nucleotide edits for both arrays using reference amplicons of known edit state (Fig. 5e). We then quantified edit levels across the 12 target sites in barcode arrays of WNT-BC1 cells (three replicates under the editing condition) and in transfected BC2-only cells (Fig. 5e and Extended Data Fig. 7c). Edit levels at each site were at least 17 times higher under the editing condition than under control conditions, while variation across sites was relatively low (standard deviation of 0.088 for the BC1 array and 0.057 for the BC2 array). BC1 showed a slight positional bias favoring edits distal to the phage promoter, whereas BC2 exhibited a more uniform distribution (Extended Data Fig. 7c). Combined with earlier results (Fig. 1e and Extended Data Fig. 1c), our analysis shows that writing and reading of edits are largely insensitive to barcode position within an array. We also found that almost all possible combinations of barcode edits are obtained during recording, and no single combination dominates the outcomes (Fig. 5f and Extended Data Fig. 7d), further confirming that INSCRIBE efficiently uses its full memory capacity.

INSCRIBE memory is sufficient for accurate reconstruction

INSCRIBE cell lines benefit from multiple genomic integrations of barcode arrays, each providing an independent measurement of base editor activity in a cell. To understand how memory capacity influences reconstruction accuracy, we simulated the process of writing and reading edits based on our experimental results (Methods). Base editing is a probabilistic process at the single-nucleotide level, with each target site having an editing probability proportional to the signaling activity in the cell. Assuming uniform edit probabilities across 12 sites per array (Fig. 5e), we modeled single-array editing as a binomial process and varied the editing probability from 0 to 1 in 0.01 increments. We then simulated cells containing 1 to 10 barcode array integrations by applying the same editing probability to all arrays within a cell and mimicked the readout process using synthetic barcode array datasets derived from experimental BC1 images (Fig. 1). Our simulation showed a linear correlation between the inferred and true editing probabilities (Extended Data Fig. 8a). Increasing the number of barcode arrays per cell enhanced this correlation, indicating improved reconstruction accuracy (Extended Data Fig. 8a,b). However, there are diminishing returns beyond three barcode arrays. Notably, the number of barcode array integrations in WNT and BMP INSCRIBE cell lines is within the range required for accurate single-cell reconstruction of signaling activity (Extended Data Fig. 8c).

Multiple barcode array integrations can also introduce recording noise if arrays at different genomic loci are edited with slightly different rates. To assess this noise, we compared empirical and simulated results from each INSCRIBE cell line (Extended Data Fig. 8d–f). Variability in recovered edit levels was evaluated relative to the mean barcode edit level per cell. We first established a baseline for the readout noise, resulting solely from the ratiometric readout process, using cells with known edit states (Fig. 1 and Extended Data Fig. 1), where all synthetic barcode arrays in a cell have the identical number of edits. For any given edit level, experimental variability exceeded this baseline readout noise. Part of this additional variation can be attributed to inherent sampling differences, as each barcode array may contain

https://doi.org/10.1038/s41589-026-02168-3

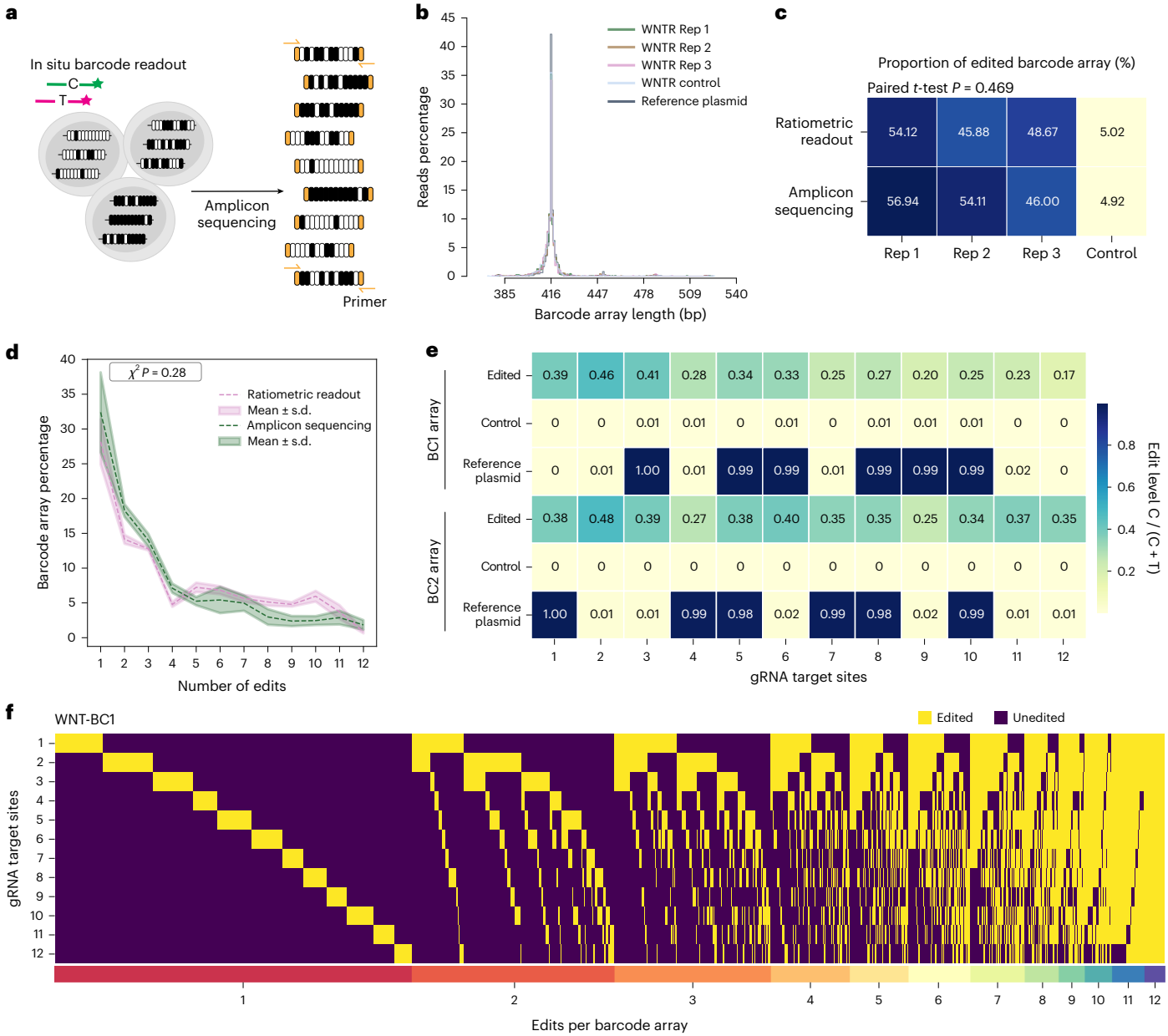

Fig. 5 | Evaluating genomic stability and edit patterns of INSCRIBE barcode arrays by sequencing. a, WNT-BC1 or BC2-only cells from the same population were subjected to imaging-based ratiometric readout and amplicon sequencing. WNT-BC1 recordings were induced by 500 ng ml^{-1} Dox, 10 μM TMP and 3 μM CHIR for 3 days. BC2 recordings were induced by co-transfection of CMV-ABEMax plasmid and CAG-sgRNA plasmid. **b**, Histogram of barcode array lengths recovered from amplicon sequencing for WNT-BC1 cells after recording (three biological replicates) and an unstimulated control population maintained in culture for over 1 year. The length distribution for the barcode array amplified from a plasmid is included as a reference. **c**, Heat map showing the proportion of edited barcode arrays recovered from ratiometric readout and amplicon sequencing. Edited arrays in imaging-based analyses are identified as those with CNN-predicted edit levels above the 95th percentile of arrays in the unstimulated control condition. The paired two-sided *t*-test *P* value across the replicates from ratiometric readout and amplicon sequencing is shown. **d**, Distribution of edit numbers in edited barcode arrays based on ratiometric readout (pink) and amplicon sequencing (green). For imaging-based analysis, the CNN output is binned into 12 classes. The shaded areas represent the mean ± s.d. across three biological replicates. The two-sided χ^2 *P* value between the distribution from ratiometric readout and amplicon sequencing is shown. **e**, Heat map of edit level for each gRNA target site in the BC1 and BC2 array under edited and control conditions, as recovered from amplicon sequencing. Analysis of reference plasmids with known edit statuses ('001011011100' for the BC1 array and '100110110100' for the BC2 array) demonstrates the single-bp accuracy of long-read amplicon sequencing. **f**, Edit status of all edited barcode arrays recovered by amplicon sequencing from three biological replicates of WNT-BC1 recording experiments.

a different number of edited sites even when all share the same editing probability. We captured this aspect of the recording noise by simulating cells with integration counts mirroring cells in our experiments (Extended Data Fig. 8c) and applying the same readout noise. The remaining unexplained variation can be attributed to varying edit probabilities of arrays at different genomic loci, which we modeled by adding normally distributed noise to each cell's overall edit probability, generating a slightly different edit probability for each array within the cell.

Our analysis showed that readout noise contributed minimally to overall variability. For WNT-BC1 and BMP-BC1, the empirical variance matched simulations incorporating normally distributed noise

with standard deviations of 0.21 and 0.28, respectively (Extended Data Fig. 8d,e), indicating that different barcode array integrations in these cells are edited at different rates. By contrast, observed variance in BMP-BC2 cells had considerable overlap with simulations assuming equal edit probability for all barcode arrays (Extended Data Fig. 8f), and a modest normal noise with a standard deviation of 0.09 was sufficient to match the experimental results. Therefore, the positional effect of genomic integration on BC2 appears to be weaker than BC1, potentially due to higher accessibility of BC2 integrations or sequence-specific differences between gRNAs.

INSCRIBE reveals persistent cellular memory in the BMP pathway

Cell-to-cell variability is a fundamental feature of biological systems, enabling a range of outcomes that influence adaptability and function[40,41]. Variability is particularly important in signaling, where differences in cellular responses can influence developmental processes and tissue organization. Even in a genetically identical population, individual cells can display a wide range of behaviors in response to the same stimuli[42]. Such variability could arise from the stochastic nature of protein expression[43,44] and regulatory features of the signaling pathways[45,46]. However, the functional consequences of cellular variability are often difficult to identify because it requires linking the initial heterogeneity to an eventual phenotype. By recording signaling activity into the genome, INSCRIBE provides a way to establish this connection.

Using the INSCRIBE cell lines, we explored whether initial heterogeneity in pathway activity results in persistent differences in how cells respond to subsequent stimulations. We examined cells exposed to BMP or WNT signals twice, with varying time intervals between exposures (Fig. 6a). The initial response was recorded in the genome as barcode edits, which are inherited by progeny cells. Recording was then disabled, and the magnitude of the second response was measured by H2B–CFP accumulation. We asked whether the magnitudes of the first and second responses were correlated and how this correlation evolved over time. Correlation in this context signifies a memory of the past response level, which persists over several cell generations.

For both pathways, H2B–CFP produced during the first exposure was diluted to a consistent low baseline within 3 days after signal withdrawal (Extended Data Fig. 9a–c, green), and a second stimulation led to elevated H2B–CFP levels (Extended Data Fig. 9a–c, pink), indicating that the endpoint CFP intensity reflects only the magnitude of the second response. Similarly, we confirmed that barcode edits capture only the initial response level by demonstrating that edit levels remained unchanged after the second stimulation, as no Dox and TMP were added to induce recording during this phase (Extended Data Fig. 9d–f). This allowed us to measure the amplitude of response to the first and second stimulations separately.

We then examined the correlation between the first and second response levels at the single-cell level. As anticipated from our earlier results (Fig. 2 and Extended Data Fig. 3), immediately after 3 days of CHIR for WNT-BC1 cells, 3 days of BMP2 for BMP-BC1 cells and 2 days of BMP2 for BMP-BC2 cells, there was a strong correlation between CFP and edit levels, whether inferred from intensity ratio or the CNN model (Fig. 6b). For the WNT pathway, the correlation between the magnitudes of the first and second responses declined rapidly and consistently as the interval between the two stimulations increased from 3 to 18 days (Fig. 6b,d). Remarkably, the BMP pathway exhibited distinct and reproducible dynamics across both arrays (Fig. 6b). The correlation remained nearly steady, fluctuating between 0.4 and 0.5, for stimulations up to 18 days apart and declined only for intervals beyond 3 weeks. To test if cells with low reporter activity and therefore little recording have affected our analysis, we carefully controlled for cells with both edit levels and H2B–CFP intensities below the 95th percentile of unstimulated controls. In total, 99.9% of WNT-BC1, 98.9% of BMP-BC1 and 100% of BMP-BC2 cells were above this threshold (Fig. 6c), indicating negligible contribution from silenced cells. Importantly, the contrasting memory dynamics, rapid decay for WNT and persistent memory for BMP were evident regardless of whether or not these low-responding cells were included in the analysis (Fig. 6b and Extended Data Fig. 9g).

This finding reveals that activation of the BMP pathway induces a lasting cellular memory. Descendants of cells that exhibit a strong BMP response tend to maintain an elevated responsiveness to subsequent BMP stimulation, even up to 18 days later (Fig. 6e and Extended Data Fig. 9h). This phenomenon cannot be attributed to genetic differences between cells, as the observed memory effect dissipates by 26 days after the initial exposure.

Discussion

The fate of a cell is impacted by factors such as lineage and signaling history that are often inaccessible to direct observation. Programming cells to chronicle their molecular history in their genome over time has emerged as a promising solution to this fundamental problem[25–27]. Here, we introduce INSCRIBE, a new approach to imaging-based molecular recording that infers past signaling activity in individual cells from endpoint measurements, without the need for sequential imaging. INSCRIBE permanently records the signaling activity level over a specified time, or the duration of signaling with a known intensity, as a set of single base edits in genomic barcode arrays. The fraction of edited sites can be detected at a later time using ratiometric barcode readout, which only requires ordinary fluorescence microscopy with two channels for each signal of interest.

We tested INSCRIBE in HEK293 and mES cell lines engineered to record the activity of either the BMP or WNT pathway. Unlike reporter systems that monitor pathway activity by expressing a fluorescent protein, INSCRIBE captures pathway activity as DNA mutations that are stably inherited through cell divisions and unaffected by fluctuations in translation or protein turnover. In principle, INSCRIBE's recording capabilities are not restricted to transcriptional regulation of gRNA through CREs; any signal that can be converted into a proportional change in edit rate can be recorded and read out similarly. For example, future work could link the edit rate to endogenous protein levels by fusing Cas9 to conditionally stable nanobodies[47].

Using INSCRIBE, we discovered a persistent memory in the BMP pathway, evidenced by the correlation between response levels to two stimulations occurring up to 18 days apart. To our knowledge, this phenomenon has not been previously reported, which raises intriguing questions regarding its underlying mechanism and biological importance. Developmental signaling pathways, including BMP, are repeatedly deployed to regulate various processes such as growth, differentiation and morphogenesis throughout different stages of development. We speculate that memory of past signaling activity could serve to coordinate these diverse aspects of tissue development. For instance, an initial signal gradient might direct cell fate decisions, whereas a later uniform signal promotes proliferation. By retaining the memory of the initial response, the system can fine-tune the population sizes of different cell types, ensuring proper tissue development and organization.

While INSCRIBE offers an innovative solution for recording signaling activity, its current implementation also has several limitations that need to be considered. First, INSCRIBE only records cumulative signaling activity, making it difficult to distinguish between an intense, short-lived signal and a lower-intensity, sustained signal. Temporal control of recording using inducible ABE can partially address this issue by allowing recordings over different time windows to probe signaling dynamics. Second, for endogenous inputs, dynamic range can present a constraint. Basal pathway activity, feedback, adaptation and cell-to-cell heterogeneity in native contexts may saturate a fast recorder or leave a slow one below threshold. Accordingly, INSCRIBE's dynamic range should be calibrated to the expected signal amplitude

https://doi.org/10.1038/s41589-026-02168-3

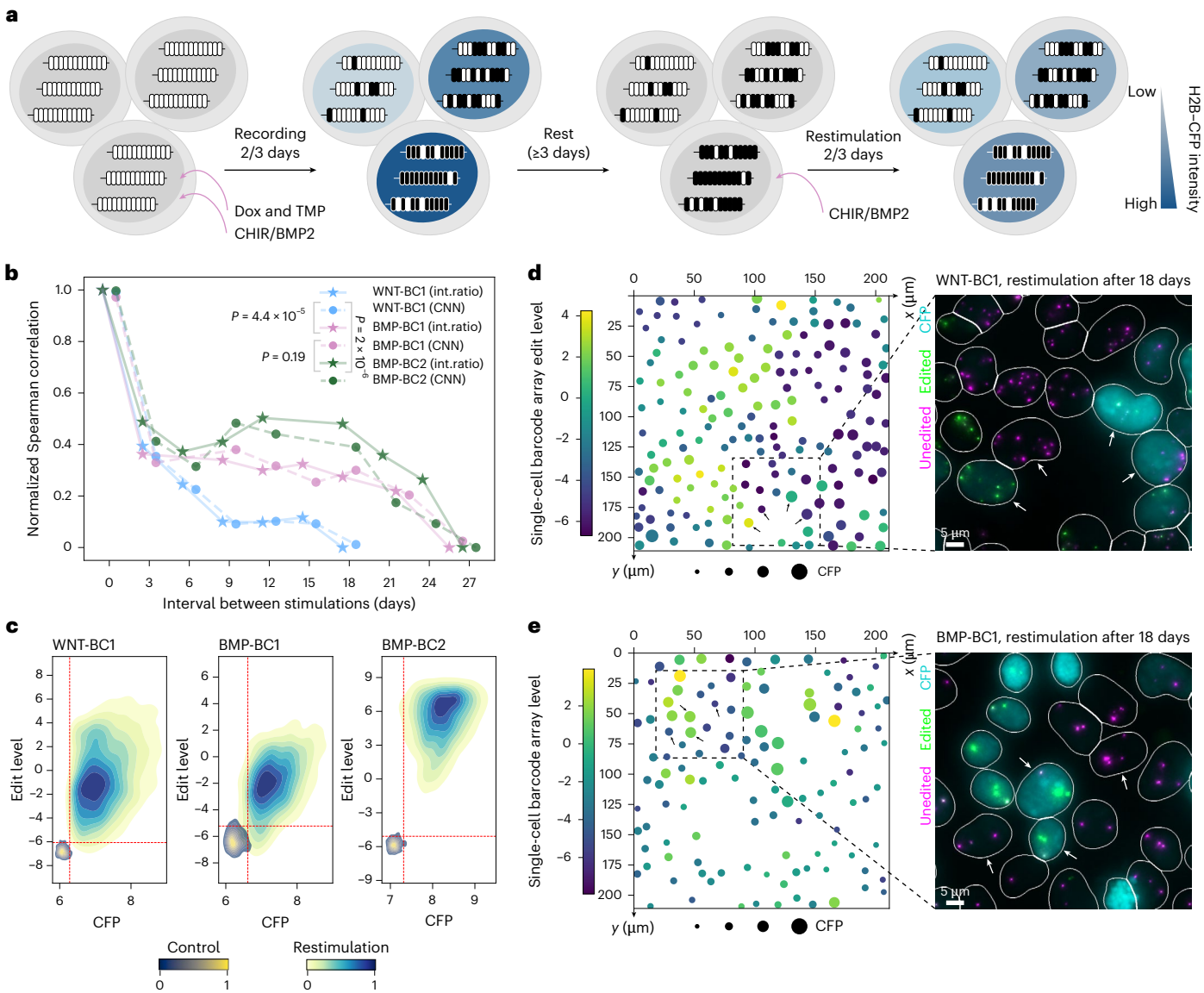

Fig. 6 | Enduring effects of cell-to-cell variability in response to WNT and BMP signals. a, WNT-BC1, BMP-BC1 and BMP-BC2 cells were exposed to 3 µM CHIR for 3 days, 256 ng ml^{-1} BMP2 for 3 days and 64 ng ml^{-1} BMP2 for 2 days, respectively, twice with different time intervals in between. Recording was induced only during the first stimulation using Dox (100 ng ml^{-1} for WNT, 500 ng ml^{-1} for BMP) and 10 µM TMP. **b**, Normalized Spearman correlation between the first and second response levels for WNT-BC1 (blue), BMP-BC1 (pink) and BMP-BC2 (green) across time intervals. The first response level was measured either by intensity ratio (solid line) or the CNN model (dashed line). The second response level was measured by H2B–CFP intensity. Spearman correlations were normalized to the maximum and minimum values for each line across time intervals. Two-sided *F*-tests were performed on normalized Spearman correlations over time after cubic polynomial regressions, with FDR-adjusted *P* values indicated. **c**, Two-dimensional kernel density estimation plots display the joint distribution of single-cell edit and CFP levels for WNT-BC1, BMP-BC1 and BMP-BC2. Edit level was calculated as the average intensity ratio across all barcode arrays in each cell. Color bars indicate relative two-dimensional kernel density estimation density for the control and stimulated groups (data from **b**). Red lines indicate the 95th percentile of edits and CFP level in control groups. **d**,**e**, Spatial context in representative fields of view for WNT-BC1 (**d**) and BMP-BC1 (**e**) restimulated after 18 days. Each point marks a cell centroid, with size being proportional to H2B–CFP intensity and color indicating edit level. Right: microscopy image with arrows highlighting cells exhibiting weak or strong second responses. Edit level was calculated as the average of intensity ratios across all barcode arrays in each cell. Nuclei are outlined for clarity.

and recording window. Different barcode arrays exhibit distinct edit rates depending on their gRNA sequences, and suboptimal gRNAs can be used to fine-tune the edit rate of a given barcode array; higher edit rates suit weak or brief signals, whereas lower rates suit strong or prolonged signals[48]. Finally, ABE expression may interfere with some cellular processes through gRNA-independent off-target editing of RNA transcripts[49]. Therefore, modified ABE variants with reduced RNA off-target activity may be better suited for sensitive applications.

In summary, INSCRIBE provides a versatile, scalable and quantitative method for genetic recording of biological signals with in situ readout. The detection of barcode edits is greatly simplified by ratiometric readout, offering a faster, cheaper and more straightforward approach than both sequencing- and imaging-based alternatives. Looking ahead, INSCRIBE is poised to be readily adaptable to a wide variety of developmental systems and disease models. Orthogonal barcode arrays, like the two developed and characterized here, can be used concurrently to simultaneously record multiple signals. Endpoint analysis of cells can be integrated with spatial multiomics to create enhanced cell atlases that combine past signaling activity, spatial information, gene expression, chromosomal architecture and chromatin states[50].

By connecting past molecular events to their future outcomes across cells, tissues and individuals, INSCRIBE will empower development of predictive models of biological processes and pave the way for new strategies to control and manipulate cell fate.

Online content

Any methods, additional references, Nature Portfolio reporting summaries, source data, extended data, supplementary information, acknowledgements, peer review information; details of author contributions and competing interests; and statements of data and code availability are available at https://doi.org/10.1038/s41589-026-02168-3.

References

1. Liberali, P. & Schier, A. F. The evolution of developmental biology through conceptual and technological revolutions. *Cell* **187**, 3461–3495 (2024).
2. Briscoe, J. & Small, S. Morphogen rules: design principles of gradient-mediated embryo patterning. *Development* **142**, 3996–4009 (2015).
3. Ribes, V. & Briscoe, J. Establishing and interpreting graded sonic hedgehog signaling during vertebrate neural tube patterning: the role of negative feedback. *Cold Spring Harb. Perspect. Biol.* **1**, a002014 (2009).
4. Marchingo, J. M. et al. T cell signaling. Antigen affinity, costimulation, and cytokine inputs sum linearly to amplify T cell expansion. *Science* **346**, 1123–1127 (2014).
5. Anastas, J. N. & Moon, R. T. WNT signalling pathways as therapeutic targets in cancer. *Nat. Rev. Cancer* **13**, 11–26 (2013).
6. Ishiguro, S., Mori, H. & Yachie, N. DNA event recorders send past information of cells to the time of observation. *Curr. Opin. Chem. Biol.* **52**, 54–62 (2019).
7. Kretzschmar, K. & Watt, F. M. Lineage tracing. *Cell* **148**, 33–45 (2012).
8. Roquet, N., Soleimany, A. P., Ferris, A. C., Aaronson, S. & Lu, T. K. Synthetic recombinase-based state machines in living cells. *Science* **353**, aad8559 (2016).
9. Chow, K.-H. K. et al. Imaging cell lineage with a synthetic digital recording system. *Science* **372**, eabb3099 (2021).
10. Farzadfard, F. & Lu, T. K. Synthetic biology. Genomically encoded analog memory with precise in vivo DNA writing in living cell populations. *Science* **346**, 1256272 (2014).
11. Kalhor, R., Mali, P. & Church, G. M. Rapidly evolving homing CRISPR barcodes. *Nat. Methods* **14**, 195–200 (2017).
12. Perli, S. D., Cui, C. H. & Lu, T. K. Continuous genetic recording with self-targeting CRISPR–Cas in human cells. *Science* **353**, aag0511 (2016).
13. Loveless, T. B. et al. Lineage tracing and analog recording in mammalian cells by single-site DNA writing. *Nat. Chem. Biol.* **17**, 739–747 (2021).
14. McKenna, A. et al. Whole-organism lineage tracing by combinatorial and cumulative genome editing. *Science* **353**, aaf7907 (2016).
15. Frieda, K. L. et al. Synthetic recording and in situ readout of lineage information in single cells. *Nature* **541**, 107–111 (2017).
16. Sheth, R. U., Yim, S. S., Wu, F. L. & Wang, H. H. Multiplex recording of cellular events over time on CRISPR biological tape. *Science* **358**, 1457–1461 (2017).
17. Shipman, S. L., Nivala, J., Macklis, J. D. & Church, G. M. Molecular recordings by directed CRISPR spacer acquisition. *Science* **353**, aaf1175 (2016).
18. Bhattarai-Kline, S. et al. Recording gene expression order in DNA by CRISPR addition of retron barcodes. *Nature* **608**, 217–225 (2022).
19. Farzadfard, F. et al. Single-nucleotide-resolution computing and memory in living cells. *Mol. Cell* **75**, 769–780 (2019).
20. Tang, W. & Liu, D. R. Rewritable multi-event analog recording in bacterial and mammalian cells. *Science* **360**, eaap8992 (2018).
21. Chadly, D. M. et al. Reconstructing cell histories in space with image-readable base editor recording. Preprint at *bioRxiv* https://doi.org/10.1101/2024.01.03.573434 (2024).
22. Choi, J. et al. A time-resolved, multi-symbol molecular recorder via sequential genome editing. *Nature* **608**, 98–107 (2022).
23. Chen, W. et al. Symbolic recording of signalling and *cis*-regulatory element activity to DNA. *Nature* **632**, 1073–1081 (2024).
24. Loveless, T.B. et al. Open-ended molecular recording of sequential cellular events into DNA. *Nat. Chem. Biol.* **21**, 512–521 (2025).
25. Sheth, R. U. & Wang, H. H. DNA-based memory devices for recording cellular events. *Nat. Rev. Genet.* **19**, 718–732 (2018).
26. Farzadfard, F. & Lu, T. K. Emerging applications for DNA writers and molecular recorders. *Science* **361**, 870–875 (2018).
27. Lear, S. K. & Shipman, S. L. Molecular recording: transcriptional data collection into the genome. *Curr. Opin. Biotechnol.* **79**, 102855 (2023).
28. Wagner, D. E. & Klein, A. M. Lineage tracing meets single-cell omics: opportunities and challenges. *Nat. Rev. Genet.* **21**, 410–427 (2020).
29. Askary, A. et al. The lives of cells, recorded. *Nat. Rev. Genet.* **26**, 203–222 (2025).
30. MacDonald, B. T., Tamai, K. & He, X. Wnt/β-catenin signaling: components, mechanisms, and diseases. *Dev. Cell* **17**, 9–26 (2009).
31. Katagiri, T. & Watabe, T. Bone morphogenetic proteins. *Cold Spring Harb. Perspect. Biol.* **8**, a021899 (2016).
32. Askary, A. et al. In situ readout of DNA barcodes and single base edits facilitated by in vitro transcription. *Nat. Biotechnol.* **38**, 66–75 (2020).
33. Korchynskyi, O. & ten Dijke, P. Identification and functional characterization of distinct critically important bone morphogenetic protein-specific response elements in the *Id1* promoter. *J. Biol. Chem.* **277**, 4883–4891 (2002).
34. Korinek, V. et al. Constitutive transcriptional activation by a β-catenin–TCF complex in $APC^{-/-}$ colon carcinoma. *Science* **275**, 1784–1787 (1997).
35. Eng, C.-H. L. et al. Transcriptome-scale super-resolved imaging in tissues by RNA seqFISH+. *Nature* **568**, 235–239 (2019).
36. Chen, K. H., Boettiger, A. N., Moffitt, J. R., Wang, S. & Zhuang, X. Spatially resolved, highly multiplexed RNA profiling in single cells. *Science* **348**, aaa6090 (2015).
37. Teague, S. et al. Time-integrated BMP signaling determines fate in a stem cell model for early human development. *Nat. Commun.* **15**, 1471 (2024).
38. Raj, B. et al. Simultaneous single-cell profiling of lineages and cell types in the vertebrate brain. *Nat. Biotechnol.* **36**, 442–450 (2018).
39. Gaudelli, N. M. et al. Programmable base editing of A•T to G•C in genomic DNA without DNA cleavage. *Nature* **551**, 464–471 (2017).
40. Altschuler, S. J. & Wu, L. F. Cellular heterogeneity: do differences make a difference? *Cell* **141**, 559–563 (2010).
41. Niepel, M., Spencer, S. L. & Sorger, P. K. Non-genetic cell-to-cell variability and the consequences for pharmacology. *Curr. Opin. Chem. Biol.* **13**, 556–561 (2009).
42. Mitchell, S. & Hoffmann, A. Identifying noise sources governing cell-to-cell variability. *Curr. Opin. Syst. Biol.* **8**, 39–45 (2018).
43. Elowitz, M. B., Levine, A. J., Siggia, E. D. & Swain, P. S. Stochastic gene expression in a single cell. *Science* **297**, 1183–1186 (2002).
44. Ozbudak, E. M., Thattai, M., Kurtser, I., Grossman, A. D. & van Oudenaarden, A. Regulation of noise in the expression of a single gene. *Nat. Genet.* **31**, 69–73 (2002).
45. Snijder, B. & Pelkmans, L. Origins of regulated cell-to-cell variability. *Nat. Rev. Mol. Cell Biol.* **12**, 119–125 (2011).

46. Sigal, A. et al. Variability and memory of protein levels in human cells. *Nature* **444**, 643–646 (2006).
47. Tang, J. C. et al. Detection and manipulation of live antigen-expressing cells using conditionally stable nanobodies. *eLife* **5**, e15312 (2016).
48. Zhang, C. et al. Prediction of base editor off-targets by deep learning. *Nat. Commun.* **14**, 5358 (2023).
49. Grünewald, J. et al. Transcriptome-wide off-target RNA editing induced by CRISPR-guided DNA base editors. *Nature* **569**, 433–437 (2019).
50. Takei, Y. et al. Integrated spatial genomics reveals global architecture of single nuclei. *Nature* **590**, 344–350 (2021).

Methods

Design of INSCRIBE barcode arrays

INSCRIBE barcode arrays are made of 12 identical barcodes, each 31 bp long, that are assembled together by Golden Gate assembly. Each barcode includes a 20-bp probe site that partially overlaps with a 20-bp gRNA target site. Each gRNA target site was designed to contain only one editable A nucleotide within the activity window of ABE[51] to ensure that edit outcomes are pure and predictable. Probe sequences were designed with 50% GC content and a predicted melting temperature between 56 and 60 °C. We also avoided recognition sites of certain restriction enzymes (BsaI, BsmBI, BpiI, AarI and XbaI) within the memory arrays to facilitate cloning. Identification of individual barcodes within an array in sequencing data is facilitated by unique 4-bp cloning scars flanking each barcode. BC1 and BC2 arrays share the same overall architecture, including barcode length, number of barcodes, flanking regulatory elements and the mode of genomic integration. The barcode sequence of the BC1 array is 5′-ATCAGGGCGTGTATGTTGACGAATC ACAGGG-3′, and the barcode sequence of the BC2 array is 5′-ATC GCCGAAGGGATTGGTATCTGAACAGCGG-3′.

Plasmid construction

The sequences of plasmids, probes and constructs used in this study are listed in Supplementary Data Set 1. All plasmids were sequence verified by full plasmid sequencing (Plasmidsaurus). Annotated SnapGene files of the INSCRIBE components, CMV-ABEMax, CAG-gRNA and the reference plasmids used for amplicon sequencing are available in the Zenodo repository associated with this paper[52]. The file names match those listed in Supplementary Data Set 1.

The Dox-inducible system was designed as an all-in-one plasmid with PiggyBac inverted terminal repeats and was synthesized by VectorBulider. ABEMax[53] (Addgene, 112095) was driven by a tet-responsive promoter (TRE3G)[54]. The modified rtTA (TetOn 3G) was constitutively expressed by the *EF1A* promoter and was followed by self-cleaving P2A peptide and the puromycin resistance gene. The degron[55] was synthesized as a gBlock by Integrated DNA Technologies and inserted downstream of ABEMax within the same open reading frame, following a 3× GGGS linker.

gRNAs targeting all 12 barcodes of each barcode array were integrated downstream of the H2B–CFP coding region, spaced by the triple helix sequence to stabilize the H2B–CFP mRNA that lacks the poly(A) tail after self-cleavage[56]. The gRNA sequence was flanked by hammerhead and hepatitis delta virus ribozymes[56] to release gRNA from transcripts that also encode H2B–CFP. The triple helix–gRNA–ribozyme sequences were synthesized as gBlocks by Integrated DNA Technologies and integrated into the target site using a HiFi DNA Assembly Cloning kit (New England Biolabs, M5520). WNT- and BMP-responsive promoters were used to drive the expression of the H2B–CFP-gRNA constructs. These plasmids included hygromycin resistance for subsequent selection.

All 12 barcodes and the T3 promoter were synthesized as single-stranded DNA by Integrated DNA Technologies, annealed to make double-stranded DNA and assembled together in one reaction with BsaI restriction enzymes and Golden Gate Assembly (New England Biolabs, E1601). The inserts possessed BsaI restriction sites at both ends in the proper orientation, each followed by a 4-bp sequence to achieve ordered assembly. The handles for the inserted barcode sites from 1 to 12 and T3 promoter are TGCC–GCAA, GCAA–ACTA, ACTA–TTAC, TTAC–CAGA, CAGA–TGTG, TGTG–GAGC, GAGC–AGGA, AGGA–ATTC, ATTC–CGAA, CGAA–ATAG, ATAG–AAGG, AAGG–AACT and AACT–ACCG.

Cell culture

HEK293 (ATCC, CRL-1573) cells were cultured in DMEM (Gibco, 11960069) supplemented with 10% fetal bovine serum (PEAK, PS-FB4) and 1× penicillin–streptomycin–L-glutamine (Gibco, 10378016) on polystyrene plates at 37 °C with 5% CO_2. For routine passaging, the growth medium was removed, cells were briefly washed with 1× PBS (Gibco, 14190250), and 0.05% trypsin (Gibco, 25-300-120) was added and incubated at 37 °C with 5% CO_2 for 5 min. Trypsin was then neutralized with growth medium at room temperature. The cells were centrifuged for 5 min at 300*g*, the supernatant was discarded, and the cell pellet was resuspended in fresh growth medium. The cells were then reseeded into new tissue culture plates for subsequent cell culture. Notably, WNT activation has been shown to promote HEK293 proliferation and protect against serum starvation-induced apoptosis[57], so we minimized any confounding effects by matching seeding density and carefully monitoring cell viability throughout the experiments.

mES cells (female, pSM44) were seeded on six-well polystyrene plates that were coated with 0.2% (wt/vol) gelatin (Sigma, G1393) at 37 °C for 30 min and cultured in N2B27/2iLIF medium consisting of 50% DMEM/F-12 (Gibco, 11330032), 50% Neurobasal medium (Gibco, 21103049), 2% B-27 supplement (Gibco, 17504044), 1% N-2 supplement (Gibco, 17502048), 0.1 mM 2-mercaptoethanol (Sigma, M3148) and 2 mM L-glutamine (Gibco, 25030081), supplemented with 3 µM CHIR (Selleck Chemicals, S2924), 1 µM PD0325901 (Selleck Chemicals, S1036) and 10 ng ml^{-1} mouse leukemia inhibitory factor (Gibco, A35935), at 37 °C with 5% CO_2. The N2B27/2iLIF medium was changed daily, and the cells were passaged before reaching 75% confluency, typically every 3 days. For routine passaging, the N2B27/2iLIF medium was removed, the cells were briefly washed with 1× PBS (Gibco, 14190250), and Accutase (STEMCELL, 07920) was added and incubated at 37 °C in a 5% CO_2 incubator for 5 min. Accutase was then neutralized with FC medium at room temperature. The cells were then centrifuged for 4 min at 200*g*, the supernatant was discarded, and the cell pellet was resuspended in fresh N2B27/2iLIF medium. The cells were then reseeded into new gelatin-coated tissue culture plates for subsequent cell culture. Engineered mES cells were passaged every other day to prevent differentiation. Cell colonies were observed daily under a microscope to ensure they were round with clear boundaries. Mycoplasma screening was performed every 2 weeks.

Cell line engineering

INSCRIBE components were integrated over multiple rounds of transfection and selection. For all transfection rounds, HEK293 cells were plated in 24-well plates at a density of 200,000 cells per well 1 day before transfection and co-transfected with 400 ng of the constructs to be integrated and 100 ng of the PiggyBac transposase together with 2 µl of Lipofectamine 2000 (Invitrogen, 11668027) according to the manufacturer's instructions. One day after, the transfected cells were replated to new 24-well plates, and selection was started with corresponding antibiotics. The first layer of insertion was a series of synthetic barcode arrays, 35 cell lines for barcode array 1 and 34 cell lines for barcode array 2 to mimic the different edit statuses that may arise during recording. These cell lines were engineered in parallel and selected with 5 µg ml^{-1} blasticidin (Gibco, R21001). After the ratiometric barcode readout revealed that most cells had barcode arrays inserted, we integrated the signal-responsive gRNA reporter through a second round of transfection into the polyclonal cell lines with unedited barcode arrays and selected with 100 µg ml^{-1} hygromycin (Thermo Fisher, 10687-010). After verifying the reporter response through ligand stimulation at the cell population level, we integrated the TetOn inducible ABEMax through a third round of transfection on the top of the previous two insertions and selected with 2 µg ml^{-1} puromycin (InvivoGen, ant-pr-1). In each round of selection, the engineered cells from 1 well of a 24-well plate were expanded to 3 wells of a 6-well plate, which usually takes 2 to 3 weeks, and then frozen for subsequent experiments. Finally, we used 100 ng ml^{-1} Dox (Sigma, D9891) and 10 µM TMP (Sigma, 92131), together with 3 µM CHIR (TOCRIS, 4423) or 64 ng ml^{-1} BMP2 (R&D, 335-BM), to stimulate the polyclonal population for 3 days and detect the proportion of cells harboring all INSCRIBE components with ratiometric barcode readout, based on which we determined the total number of monoclonal lines to be screened.

For dual-barcode array cells, mES cells were plated in gelatin-coated 24-well plates at a density of 50,000 cells per well 1 day before transfection and co-transfected with 400 ng of the constructs to be integrated and 100 ng of the PiggyBac transposase together with 3 µl of Lipofectamine 3000 (Invitrogen, L3000150) according to the manufacturer's instructions. The medium was completely replaced with fresh N2B27/2iLIF after a 12-h incubation. One day after transfection, cells were subjected to selection with the corresponding antibiotics for 7 days. The INSCRIBE components were integrated as the order described above for HEK293 cells, barcode array, signal-responsive gRNA reporter and then TetOn ABEMax.

Establishing monoclonal cell lines

The final verified HEK293 polyclonal cells were trypsinized with 0.05% trypsin (Gibco, 25-300-120) at 37 °C in a 5% CO_2 incubator for 5 min. Subsequently, trypsin was neutralized with growth medium at room temperature. The cells were centrifuged for 5 min at 300*g*, the supernatant was discarded, and the cell pellet was resuspended in 1% bovine serum albumin (Cell Signaling, 9998S) in PBS. The cell suspension was then filtered through a filter cap into flow cytometry tubes and stained with 5 µl of 7-amino-actinomycin D (BD Pharmingen, 559925) per 1 million cells at 4 °C for at least 10 min. Cell sorting was then performed using a fluorescence-activated cell sorter (BD FACSAria) through the 100-µm nozzle, and 7-amino-actinomycin D-negative (viability) and H2B–CFP-negative (no leaky reporter expression) cells were gated and collected as single cells per well into 96-well plates, with four plates for each INSCRIBE cell line. Single cells were cultured in 200 µl of standard culture medium at 37 °C in a 5% CO_2 incubator, and the medium was replaced independently for each well every week.

Putative antibiotic-resistant mES cell colonies were cultured until 80% confluency. The colonies were then dissociated, counted and diluted to a density of 0.5 cells per 100 µl in N2B27/2iLIF medium. We replated the diluted cells into gelatin-coated 96-well plates at 100 µl per well. Wells with multiple colonies were marked off, and viable cells were expanded to establish monoclonal cell lines.

Once the monoclonal lines were recovered and expanded, for both HEK293 and mES cells, we used 100 ng ml^{-1} Dox (Sigma, D9891) and 10 µM TMP (Sigma, 92131), together with 3 µM CHIR (TOCRIS, 4423) or 64 ng ml^{-1} BMP2 (R&D, 335-BM), to stimulate the cells for 3 days. Ratiometric barcode readout was then used to screen the lines.

Signal recording following pathway stimulation

Dox (Sigma, D9891) was reconstituted in PBS (Gibco, 14190250) to a final concentration of 1 mg ml^{-1}. TMP (Sigma, 92131) was reconstituted in DMSO (Sigma, 276855) to a final concentration of 10 mM. CHIR (TOCRIS, 4423) was reconstituted in DMSO to a final concentration of 10 mM. BMP2 (R&D, 335-BM) was reconstituted in a buffer with 4 mM HCl (Fluka, 320331) and 0.25% bovine serum albumin (Cell Signaling, 9998S) to a final concentration of 150 µg ml^{-1}. All reagents were aliquoted and stored at −20 °C, except for BMP2, which was stored at −80 °C, thawed immediately before use and diluted with the appropriate culture medium.

For the dosage-dependent signal recording, 4,000 INSCRIBE cells were seeded on 96-well plates 1 day before stimulation, and the medium with various concentrations of ligand and Dox combinations was added to each well, followed by recording for 3 days. For recording signaling duration, 4,000 INSCRIBE cells were seeded on 96-well plates at different time points, followed by recording with constant ligand concentration the next day and ratiometric barcode readout at the same time for different durations of recording to eliminate the batch effect. For signaling memory experiments, 8,000 INSCRIBE cells were seeded on 96-well plates 1 day before stimulation. After 3 days (BC1 array) or 2 days (BC2 array) of initial stimulation and recording (with Dox and TMP), cells were split into two wells, 8,000 cells each, and cultured in medium without ligands. Every 3 days, cells were split into four wells, 8,000 cells for each. Two wells were used for the 3 days (BC1 array) or 2 days (BC2 array) of the second stimulation (without Dox and TMP) or control. The remaining two wells were maintained in culture without ligands for the next time point. The ratiometric barcode readout for different time intervals between two stimulations was performed immediately after the second stimulation. Experiments were stopped once the raw correlation values, before normalization, reached 0.2.

Ratiometric barcode readout

For ratiometric barcode readout, we seeded the cells on glass-bottom 96-well plates (Cellvis, P96-1.5H-N) that were coated with 20 µg ml^{-1} laminin (Biolamina, LN511) at 37 °C overnight. The preferred cell density was around 10,000 to 20,000 cells per well to allow straightforward segmentation while maximizing the number of cells analyzed in each field of view.

Cells were washed with 1× PBS (Gibco, 14190250), followed by fixation with a fresh mixture of methanol (Sigma, 494437) and acetic acid (Sigma, A6283). For HEK293 cells, fixation was performed with a 3:1 volume ratio at room temperature for 20 min, whereas for mES cells, a 1:1 volume ratio was applied at room temperature for 3 h. After two washes in nuclease-free water (IDT, 11-04-02-01) for 5 min each, the cells were incubated with 50 µl of T3 transcription mix consisting of 0.5 mM NTP (New England Biolabs, N0466S), 0.8 U µl^{-1} RNase inhibitor (New England Biolabs, M0314S), 5 U µl^{-1} T3 RNA polymerase (New England Biolabs, M0378S) and 1× RNAPol reaction buffer (New England Biolabs, B9012S) at 37 °C for 3 h for HEK293 cells or overnight for mES cells. After transcription, cells were fixed with fresh 4% formaldehyde solution (Thermo Scientific, 28906) in PBS for 30 min at room temperature, followed by two washes with 2× SSC (Invitrogen, 15557044) for 5 min each to remove traces of formaldehyde.

Subsequently, cells were incubated in 50 µl of prewarmed hybridization buffer, which consisted of 30% formamide (Invitrogen, AM9344), 10% dextran sulfate (Sigma, D8906) and 2× SSC at 37 °C for at least 30 min. The cells were then incubated with 4 nM Alexa Fluor 546-conjugated edited probe (Integrated DNA Technologies) and 4 nM Alexa Fluor 647-conjugated unedited probe (Integrated DNA Technologies) in 50 µl of hybridization buffer for 20 h at 37 °C. The hybridized cells were then washed four times (15 min each) at 37 °C with prewarmed wash buffer, which consisted of 30% formamide (Invitrogen, AM9344), 0.1% Triton X-100 (Sigma, T8787) and 2× SSC to remove excess probes, followed by a brief wash with 4× SSC. Nuclei were stained with 1 µg ml^{-1} DAPI (Thermo Scientific, 62248) in 4× SSC for 10 min, followed by a wash with 4× SSC for 5 min.

Immediately before imaging, 4× SSC was replaced with fresh antibleaching buffer, which consisted of 10% glucose (Sigma, G7528), 10 mM Trolox (Sigma, 238813), 1:100 diluted catalase (Sigma, C3155), 1 mg ml^{-1} glucose oxidase (Sigma, G2133) and 50 mM Tris-HCl pH 8.0 (Invitrogen, 15568025) in 4× SSC. Alternatively, the plate was stored in 4× SSC with 0.02 U µl^{-1} SUPERase RNase inhibitor (Invitrogen, AM2694) at 4 °C. Unless otherwise stated, all reagents were added at 100 µl per well.

For multiple rounds of ratiometric readout, cells after imaging were washed with 4× SSC for 5 min to remove the antibleaching buffer, followed by three washes (15 min each) at 37 °C with prewarmed stripping buffer, which consisted of 60% formamide (Invitrogen, AM9344), 0.1% Triton X-100 (Sigma, T8787) and 4× SSC. Each stripping step was followed by a brief wash in 4× SSC. Hybridization, washing and imaging procedures were then repeated as described above for subsequent barcode arrays.

Fluorescence in situ hybridization

The sequences of smFISH primary probe pools and readout probes are listed in Supplementary Data Set 1. For each primary probe, a 30- to 37-nt mRNA target region was selected, flanked on both sides by three repeats of 15-nt readout probe binding sites. The mRNA target

regions were obtained from the PaintSHOP newBalance probe set (hg38, isoform resolved)[58] and were required to satisfy the following criteria: on_target > 96%, off_target = 0, repeat_seq = 0, max_kmer < 3 and a melting temperature range from 42 to 47 °C.

For smFISH, we seeded the cells on glass-bottom 96-well plates (Cellvis, P96-1.5H-N) that were coated with 20 µg ml^{-1} laminin (Biolamina, LN511) at 37 °C overnight. The preferred cell density was around 8,000 to 10,000 cells per well to allow straightforward segmentation while maximizing the number of cells analyzed in each field of view when considering the cytoplasmic size.

Cells were washed with 1× PBS (Gibco, 14190250), followed by fixation with fresh 4% formaldehyde solution (Thermo Scientific, 28906) in PBS for 20 min at room temperature. After a wash with 1× PBS for 5 min to remove traces of formaldehyde, the cells were incubated with 70% ethanol (Sigma, 459844) for 1 h at room temperature, followed by two washes with 2× SSC (Invitrogen, 15557044) for 5 min each.

Subsequently, cells were incubated in 50 µl of prewarmed hybridization buffer, which consisted of 30% formamide (Invitrogen, AM9344), 10% dextran sulfate (Sigma, D8906), 3 mg ml^{-1} Poly(vinylsulfonic acid, sodium salt) solution (PVSA) (Sigma, 278424) and 2× SSC at 37 °C for at least 30 min. The cells were then incubated with 4 nM primary probe pool (4 nM per probe; Integrated DNA Technologies), consisting of 20 probes for *ID1*, 15 probes for *ID3*, 24 probes for *ID4* and 42 probes for *SMAD6*, in 100 µl of hybridization buffer for 20 h at 37 °C. The hybridized cells were then washed four times (15 min each) at 37 °C with prewarmed wash buffer, which consisted of 30% formamide (Invitrogen, AM9344), 3 mg ml^{-1} PVSA (Sigma, 278424) and 2× SSC, followed by a brief wash with 4× SSC containing 3 mg ml^{-1} PVSA.

For cycles of readout probe hybridization and imaging, with the order of *ID1* and *ID3* for the first round, *ID4* and *SMAD6* for the second round and *ID3* (rehybridization control) for the third round, fluorescent readout probes (Integrated DNA Technologies) were hybridized at 50 nM each in readout buffer, consisting of 10% Ethylene carbonate (Sigma, E26258), 10% dextran sulfate (Sigma, D4911) and 2× SSC for 30 min at room temperature. Cells were then washed with 10% wash buffer, which consisted of 10% formamide (Invitrogen, AM9344), 3 mg ml^{-1} PVSA (Sigma, 278424) and 4× SSC, followed by a brief wash with 4× SSC containing 3 mg ml^{-1} PVSA. Cytoplasma and nuclei were stained with 1 µg ml^{-1} WGA-647 (Thermo Scientific, W32466) and 1 µg ml^{-1} DAPI (Thermo Scientific, 62248) in 4× SSC for 10 min, followed by a wash with 4× SSC for 5 min. Nuclei were stained in each round to facilitate image registration. Cell membranes were only stained in the third round.

Immediately before imaging, 4× SSC was replaced with fresh antibleaching buffer, which consisted of 10% glucose (Sigma, G7528), 10 mM Trolox (Sigma, 238813), 1:100 diluted catalase (Sigma, C3155), 1 mg ml^{-1} glucose oxidase (Sigma, G2133) and 50 mM Tris-HCl pH 8.0 (Invitrogen, 15568025) in 4× SSC.

After each round of imaging, cells were washed with 4× SSC for 5 min to remove the antibleaching buffer, followed by three washes (5 min each) with 55% wash buffer, which consisted of 55% formamide (Invitrogen, AM9344), 3 mg ml^{-1} PVSA (Sigma, 278424) and 4× SSC. Each stripping step was followed by a brief wash in 4× SSC. Cycles of readout probe hybridization and imaging were then repeated as described above for subsequent target mRNAs.

For smFISH combined with ratiometric readout, a heat decross-linking step was performed with 0.1 M sodium bicarbonate and 0.5 M NaCl in water at 65 °C overnight[59]. After four washes (15 min each) with 1× PBS, cells were processed following the ratiometric readout protocol described above.

Fluorescence microscopy

Cells were imaged on a Zeiss AXIO Observer Z1 inverted fluorescence microscope equipped with a Plan-Apochromat ×63/1.4-NA oil immersion objective (Zeiss), ORCA-Flash 4.0 V3 digital CMOS camera (Hamamatsu, C13440) and fluorescence lamp illuminators (X-Cite, 120PC Q). Optical sections were captured with a 21-plane *z* stack at 0.5-µm intervals to cover 10-µm thickness and ensure recovery of all barcode arrays at different *z* planes for each position. Imaging settings, including exposure times (10 ms for the DAPI channel, 50 ms for the CFP channel, 300 ms for the 546 channel, 1,000 ms for the 647 channel and 200 ms for WGA-647) were kept the same for all experiments to facilitate comparison between images. Positions were chosen solely based on the DAPI channel to avoid bias. Immersion oil with a refractive index of 1.518 (Zeiss) was used to minimize spherical aberrations.

Image processing

Images were processed using custom Python scripts.

Maximum intensity projection. To combine information across optical sections while avoiding out-of-focus slices, we assessed the focus of each *z* slice by calculating the variance of the Laplacian of the corresponding DAPI image. We then scaled these values from 0 to 100 and identified the largest stretch of slices where this normalized measure of focus is above 20. Maximum intensity projection was then applied to this stretch of *z* slices for all channels.

Registration. For experiments involving multiple rounds of imaging, images were registered using the HyperStackReg plugin in Fiji. An affine transformation model was applied to correct for translation, rotation, scaling and shear between imaging rounds. Registration was performed using the DAPI channel as a reference, as the nuclear signal provided a stable landmark across cycles.

Segmentation. For cell segmentation, we used the GPU-based 'cyto' model of CellPose3 (ref. 60), a generalist, deep learning-based cell segmentation algorithm. For the ratiometrc barcode readout analysis, segmentation was applied only to DAPI-stained nuclei to avoid incorrect segmentation of neighboring cells. For the FISH analysis, segmentation was performed on composite images combining WGA-stained cytoplasm and DAPI-stained nuclei, which improve the accuracy of cytoplasmic segmentation. Cells that intersected the border of the image were excluded from the analysis. For segmentation of barcode array spots, we manually trained classifiers through the interactive pixel classification workflow of Ilastik[61], based on one randomly picked position out of at least seven positions for each investigated condition. We then applied the classifier to the whole data set through batch processing. The probability threshold for Ilastik probability masks was set to 0.5. Any barcode array spots identified outside of cell nuclei or with the size below 3 pixels were excluded from the analysis.

Intensity measurement. After applying background subtraction with a 50-pixel rolling ball radius, the intensity of barcode array spots in each channel was obtained by integration of pixel intensity values over the segmented area of the spot. To estimate the edit level of each array, we calculated the intensity ratio, defined as the base-2 logarithm of the fluorescence intensity in the edited channel divided by the intensity in the unedited channel. Using this measure, the edit level of each cell was quantified as the average of intensity ratios for all its barcode arrays. The intensity of H2B–CFP was calculated as the natural log of average pixel intensity over the segmented nuclei.

CNN classifier training. To train the barcode classifier, we used two-channel fluorescence images of barcode array spots with known edit states. Images containing multiple spots were filtered out. The remaining images were resized, using Python's skimage package, to match the dimensions of the largest image in the dataset. Intensity values were also normalized by scaling each channel according to the maximum intensity value of that channel across the dataset.

The labels were then one-hot encoded into 13 classes corresponding to the number of possible edits. We split the dataset into training, validation and test sets, with 20% of the data reserved for testing. The remaining 80% was split further, allocating 25% for validation (resulting in an effective 60/20/20 split for training, validation and testing). For data augmentation, we applied rotation, horizontal and vertical flipping and nearest neighbor filling on the training images to enhance the model's robustness. No augmentation was applied to the validation and test data.

The CNN model comprised four convolutional layers, each with L2 regularization with a factor of 0.001 and leaky ReLU activation with an α value of 0.001. Except for the first layer, every convolutional layer is followed by two-dimensional max pooling with a 2 × 2 window and a dropout layer with a dropout rate of 0.2. The model then flattens the output from convolutional layers to feed into a dense layer, which also uses L2 regularization and leaky ReLU activation, followed by a dropout layer with a dropout rate of 0.35. Finally, the output layer consists of a single unit producing 13 output values, corresponding to the probabilities of the barcode array containing between 0 and 12 edits.

To evaluate the accuracy of ratiometric readout (Fig. 1f and Extended Data Fig. 1d), we assigned the edit number with the highest probability to each spot. By contrast, for the recording experiments, we calculated the expected value by averaging the products of each state's probability and its corresponding edit number (0 to 12).

INSCRIBE component copy number

The sequences of the quantitative PCR (qPCR) primers are listed in Supplementary Data Set 1. Genomic DNA was extracted from 1 million cells from each selected INSCRIBE monoclonal cell line using a Genomic DNA Purification kit (New England Biolabs, T3010) according to the manufacturer's instructions. In parallel, we plated 12,000 cells from each selected INSCRIBE monoclonal cell line on glass-bottom 96-well plates (Cellvis, P96-1.5H-N) coated with 20 μg ml^{-1} laminin (Biolamina, LN511) for ratiometric barcode array readout. Barcode array number was identified as the average per monoclonal cell line by ratiometric readout. TetOn-ABE and CRE-H2B–CFP-sgRNA copy number were quantified relative to the barcode array using genomic DNA qPCR.

The targeted 100-bp genomic region was amplified using iTaq Universal SYBR Green Supermix (Bio-Rad, 1725120) and primers (Integrated DNA Technologies) with a melting temperature of 60 °C, designed with PrimerQuest (Integrated DNA Technologies). We targeted the blasticidin resistance gene for the barcode array, ABEMax for TetOn-ABE and CFP for CRE-H2B–CFP-sgRNA. The input for qPCR was 10 ng of genomic DNA and 300 nM of each primer in a final reaction volume of 10 μl. The samples were incubated for 5 min at 95 °C and then 10 s at 95 °C and 30 s at 60 °C for 40 cycles. For each selected INSCRIBE monoclonal cell line, three replicates were performed, taking the average quantification cycle of each INSCRIBE component for subsequent relative quantification.

Amplicon sequencing

The sequences of primers used for amplicon sequencing are listed in Supplementary Data Set 1. For amplicon sequencing combined with ratiometric barcode array readout, 100,000 WNT-BC1 INSCRIBE cells were seeded on 24-well plates 1 day before stimulation, and 500 μl of medium with 3 μM CHIR, 500 ng ml^{-1} Dox and 10 μM TMP were added to each well, followed by recording for 3 days. BC2 array-only cells were plated in 24-well plates at a density of 200,000 cells per well 1 day before transfection and co-transfected with 296 ng of CMV-ABEMax plasmid and 123.6 ng of CAG-sgRNA plasmid with 2 μl of Lipofectamine 2000 (Invitrogen, 11668027) according to the manufacturer's instructions, followed by recording for 3 days. The recorded cells were then split to plate 12,000 cells on glass-bottom 96-well plates (Cellvis, P96-1.5H-N) coated with 20 μg ml^{-1} laminin (Biolamina, LN511) for ratiometric barcode array readout. The rest of the cells were plated on a new 24-well plate for amplicon sequencing. The next day, we performed the ratiometric barcode readout and amplicon sequencing for the cells from the same population in parallel.

Genomic DNA was extracted from WNT-BC1 INSCRIBE cells or BC2 array-only cells using a Genomic DNA Purification kit (New England Biolabs, T3010) according to the manufacturer's instructions. The targeted region was amplified from collected genomic DNA or reference plasmid using high-fidelity Herculase II Fusion DNA Polymerase (Agilent, 600675). The input template for PCR was 100 ng of genomic DNA or 1 ng of reference plasmid in a final reaction volume of 50 μl. The samples were incubated for 2 min at 95 °C; 30 s at 95 °C, 30 s at 56 °C and 60 s at 72 °C for 36 cycles and then 10 min at 72 °C. Amplicon libraries contained the barcode arrays with an extra 50 bp on each side and were sequenced by the Plasmidsaurus Premium PCR sequencing service, which is based on nanopore long-read sequencing. Raw FASTQ files were aligned to a FASTA format reference file containing the expected amplicon sequences. Alignment was performed using Bowtie 2, and subsequent analysis and data visualization were performed with custom Python scripts. We extracted base calls from each aligned read at the base editor target sites. The unique 4-bp sequences flanking each barcode were used to identify the position of barcodes in the arrays.

Barcode array writing and reading process simulation

In simulating the editing process based on our empirical findings (Fig. 5e), we assumed that the editing probability is uniform across all sites within a barcode array, leading to a binomial distribution with 12 trials. We varied the editing probability from 0 to 1, in increments of 0.01, to model different levels of signaling activity, and the same editing probability was applied for different simulated barcode arrays within the same cell. Fifty cells were simulated for each edit probability and barcode array number pair. Subsequently, we grouped barcode arrays to simulate cells containing 1 to 10 barcode array integrations.

To recreate the readout process, we paired each simulated barcode array with a real instance of the BC1 array with the same number of edits, selected randomly from images of cells with known ground truth (Fig. 1 and Extended Data Fig. 1). We then used our CNN model to classify those images and recorded the results as the observed edit level of the simulated barcode arrays. The inferred edit probability in each simulated cell was then calculated by maximum likelihood estimation based on all its barcode arrays.

Statistics and reproducibility

Biological replicates correspond to multiple monoclonal cell lines subjected to the same experimental pipeline, and all attempts at replication were successful. Representative images were selected from datasets in which three independent experiments produced consistent results.

Quantitative analyses were as defined in the figure legends. No data points were excluded unless clearly identified as technical artifacts (imaging failure, segmentation errors or cells that intersected the border), and exclusion criteria were pre-established before analysis. For all statistical tests, the type of test (one-sided or two-sided) and exact P values are provided in the figure legends. Extremely small P values below numerical precision are reported as '$P \approx 0$' to indicate values below machine-precision limits.

Randomization and blinding were not applicable. For quantitative imaging, fields of view were randomly selected based on the DAPI channel only, and an equal number of randomly chosen fields was collected for all conditions within each experiment.

Reporting summary

Further information on research design is available in the Nature Portfolio Reporting Summary linked to this article.

Data availability

The INSCRIBE barcode array amplicon sequencing datasets are deposited at the National Center for Biotechnology Information's Sequence Read Archive, under accession number PRJNA1232380. The sequences of primers, probes and constructs used in this study are listed in Supplementary Data Set 1. The exact quantified sample sizes for each experimental condition are listed in Supplementary Data Set 2. Due to the large size of the raw imaging files, public deposition in open data repositories was not feasible. However, all raw data are available from the corresponding author upon request. Source data are provided with this paper.

Code availability

All the custom scripts were written in Python Jupyter Notebook, and processed source data required to replicate our analysis and demonstration pipelines are available at Zenodo via https://doi.org/10.5281/zenodo.18307130 (ref. 52).

References

51. Anzalone, A. V., Koblan, L. W. & Liu, D. R. Genome editing with CRISPR–Cas nucleases, base editors, transposases and prime editors. *Nat. Biotechnol.* **38**, 824–844 (2020).
52. Hao, K., & Askary, A. INSCRIBE: in situ single cell recording of signal intensity as barcode edits (Version_NchB). *Zenodo* https://doi.org/10.5281/zenodo.18307130 (2026).
53. Koblan, L. W. et al. Improving cytidine and adenine base editors by expression optimization and ancestral reconstruction. *Nat. Biotechnol.* **36**, 843–846 (2018).
54. Zhou, X., Vink, M., Klaver, B., Berkhout, B. & Das, A. T. Optimization of the Tet-On system for regulated gene expression through viral evolution. *Gene Ther.* **13**, 1382–1390 (2006).
55. Iwamoto, M., Björklund, T., Lundberg, C., Kirik, D. & Wandless, T. J. A general chemical method to regulate protein stability in the mammalian central nervous system. *Chem. Biol.* **17**, 981–988 (2010).
56. Nissim, L., Perli, S. D., Fridkin, A., Perez-Pinera, P. & Lu, T. K. Multiplexed and programmable regulation of gene networks with an integrated RNA and CRISPR/Cas toolkit in human cells. *Mol. Cell* **54**, 698–710 (2014).
57. Jia, L., Miao, C., Cao, Y. & Duan, E. K. Effects of WNT proteins on cell proliferation and apoptosis in HEK293 cells. *Cell Biol. Int.* **32**, 807–813 (2008).
58. Hershberg, E. A. et al. PaintSHOP enables the interactive design of transcriptome- and genome-scale oligonucleotide FISH experiments. *Nat. Methods* **18**, 937–944 (2021).
59. Kudo, T. et al. Multiplexed, image-based pooled screens in primary cells and tissues with PerturbView. *Nat. Biotechnol.* **43**, 1091–1100 (2025).
60. Stringer, C. & Pachitariu, M. Cellpose3: one-click image restoration for improved cellular segmentation. *Nat. Methods* **22**, 592–599 (2025).
61. Berg, S. et al. Ilastik: interactive machine learning for (bio)image analysis. *Nat. Methods* **16**, 1226–1232 (2019).

Acknowledgements

We thank the members of the laboratory of A.A., especially Z. Samadi for helpful discussions and approaches for data analysis. We thank L. Sanchez-Guardado for insightful discussions. We are grateful to M. Elowitz and the Elowitz laboratory, especially M. Tran and D. Chadly, for critical feedback and for sharing plasmids with signal-responsive elements. This work was supported by a grant from the National Eye Institute (R00EY031782 to A.A.) and the University of California, Los Angeles, Eli and Edythe Broad Center of Regenerative Medicine and Stem Cell Research Transformative Technology Development Pilot Award, including support from The Rose Hills Foundation Innovator Grant Program (to A.A.).

Author contributions

A.A. and K.H conceptualized and initiated the study. K.H. and A.A. designed the study. K.H. and A.A. developed methodology. K.H., Y.L. and Y.M. performed the experiments. K.H. and A.A. generated the data. K.H., A.A., Z.S. and A.Z. analyzed and interpreted the data. K.H., A.A. and M.B. wrote the paper. A.A. and M.Z.-G. supervised the study. All authors reviewed and approved the final paper.

Competing interests

K.H and A.A. have filed a patent on recording and detection of cellular signals (The Regents of the University of California, PCT/US25/47952). The other authors declare no competing interests.

Additional information

Extended data is available for this paper at https://doi.org/10.1038/s41589-026-02168-3.

Supplementary information The online version contains supplementary material available at https://doi.org/10.1038/s41589-026-02168-3.

Correspondence and requests for materials should be addressed to Amjad Askary.

Peer review information *Nature Chemical Biology* thanks Theresa Loveless and the other, anonymous, reviewer(s) for their contribution to the peer review of this work.

https://doi.org/10.1038/s41589-026-02168-3

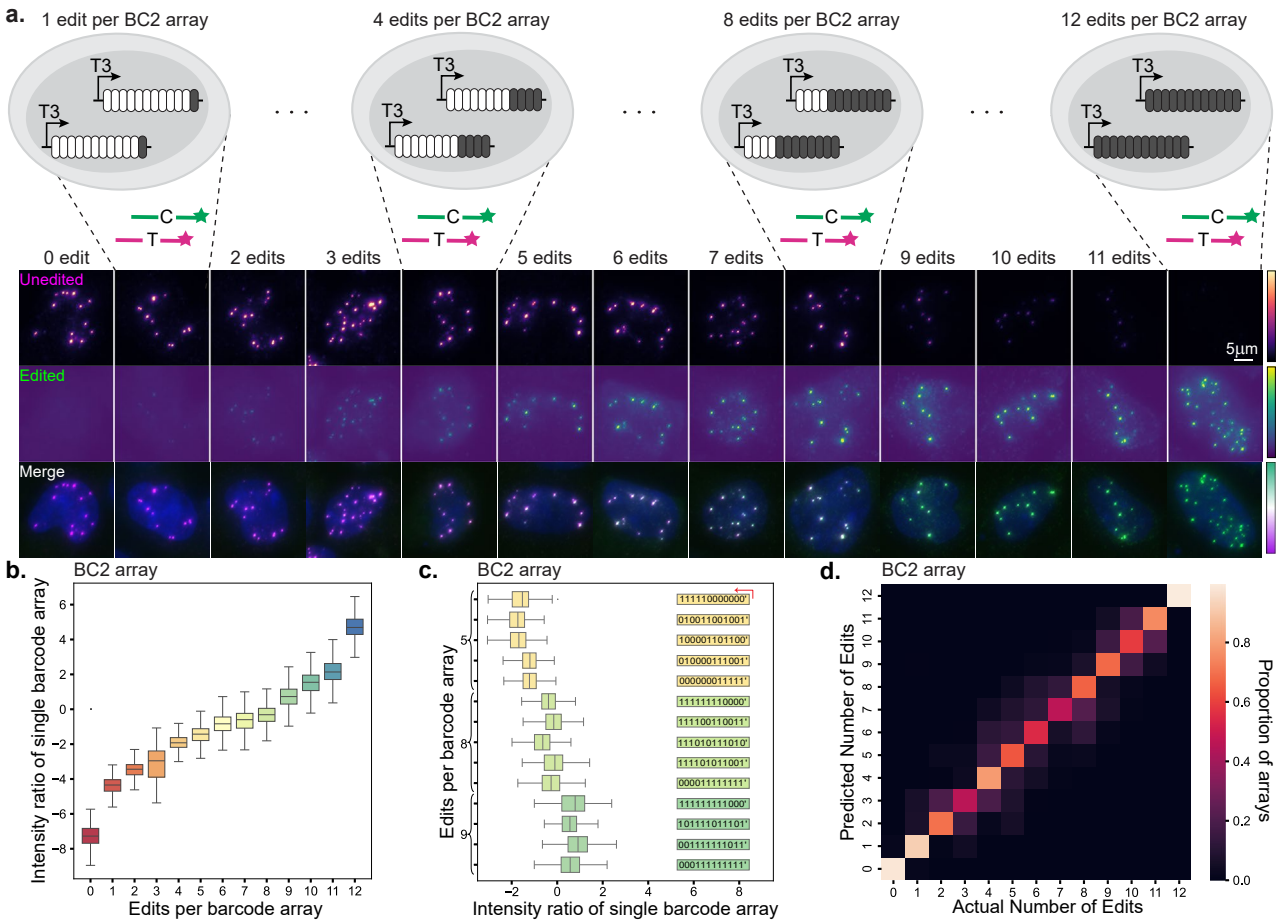

Extended Data Fig. 1 | Validation of ratiometric barcode readout for the BC2 array. a, Representative images of BC2 array cells with known edit states. Panels are organized in the same way as Fig. 1c. Each channel was contrast-adjusted using fixed display ranges (unedited: 200–12000; edited: 400–8000), as indicated by the accompanying color scales. The colour bar for merged images shown as the schematic of relative intensity (edited/unedited). **b**, Distribution of intensity ratio for each edit number of BC2 array. Boxes represent the IQR, center lines denoting medians and whiskers extending to 1.5×IQR (outliers omitted). **c**, Comparison of BC2 arrays with different edit configuration confirms that the number of edits, not their position within the array, determines intensity ratio. Boxes represent the IQR, center lines denoting medians and whiskers extending to 1.5×IQR (outliers omitted). **d**, Classification of BC2 arrays using the CNN model demonstrates accuracy comparable to that achieved for the BC1 arrays. Confusion matrix compares the true edit numbers against the predicted outputs from the CNN model. The frequency values are normalized so that each row sums to one.

https://doi.org/10.1038/s41589-026-02168-3

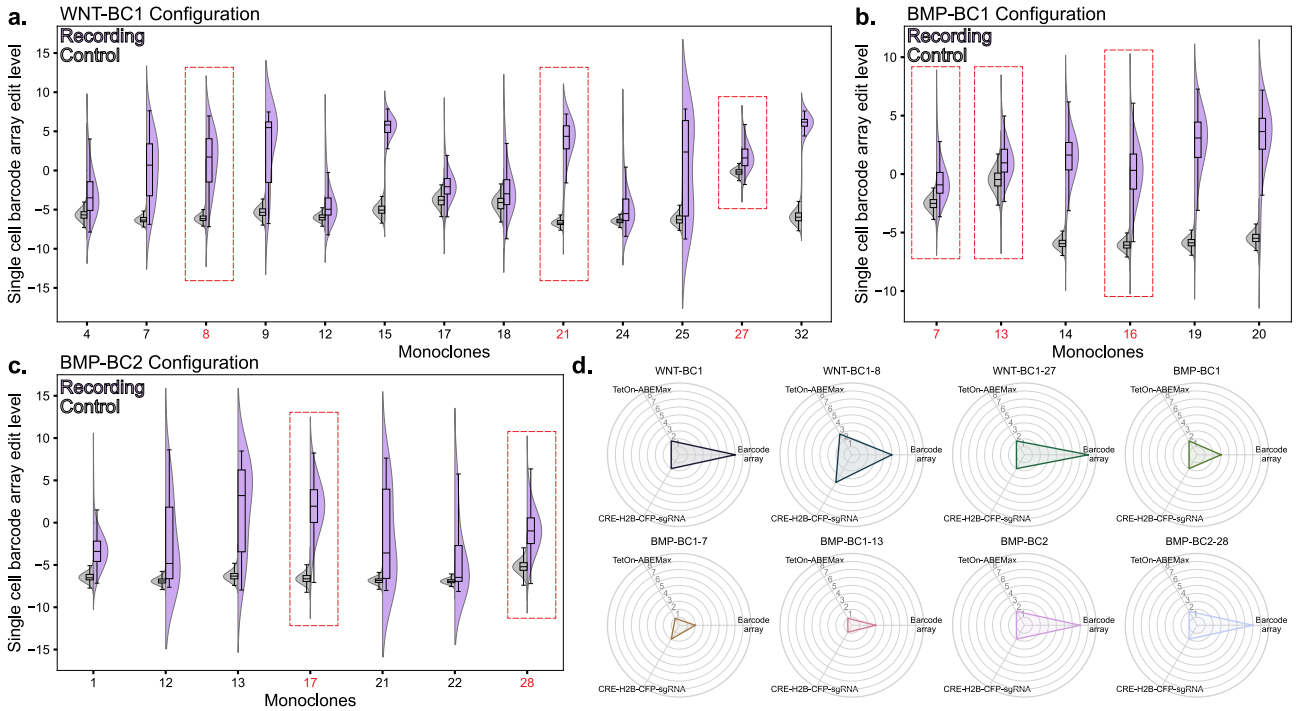

Extended Data Fig. 2 | Screening of competent monoclonal INSCRIBE cell lines. a, b and **c**, Split violin plots show the distribution of single cell edit levels after pathway stimulation compared to the unstimulated control condition for monoclonal cell lines from three INSCRIBE recording configurations, WNT-BC1 (**a**), BMP-BC1 (**b**), and BMP-BC2 (**c**). The overlaid boxes indicate the IQR, with center lines marking the median and whiskers extending to 1.5×IQR. Outliers are omitted for clarity. The WNT pathway was activated by 3 μM CHIR and the BMP pathway was activated by 64 ng/ml BMP2. The lines used for further analysis are highlighted by red dotted rectangles. **d**, Radar plots display the copy numbers of INSCRIBE components across monoclonal cell lines. Each subplot corresponds to an individual monoclonal, annotated with its INSCRIBE recording configuration and monoclonal identifier, with the exception of WNT-BC1-21, BMP-BC1-16, and BMP-BC2-17 that are abbreviated as WNT-BC1, BMP-BC1, and BMP-BC2, respectively. All the recordings were performed over 3 days with 10 μM of TMP, using 100 ng/ml of Dox for monoclonal screen. Edit level in each cell is calculated as the average of intensity ratios for all its barcode arrays.

https://doi.org/10.1038/s41589-026-02168-3

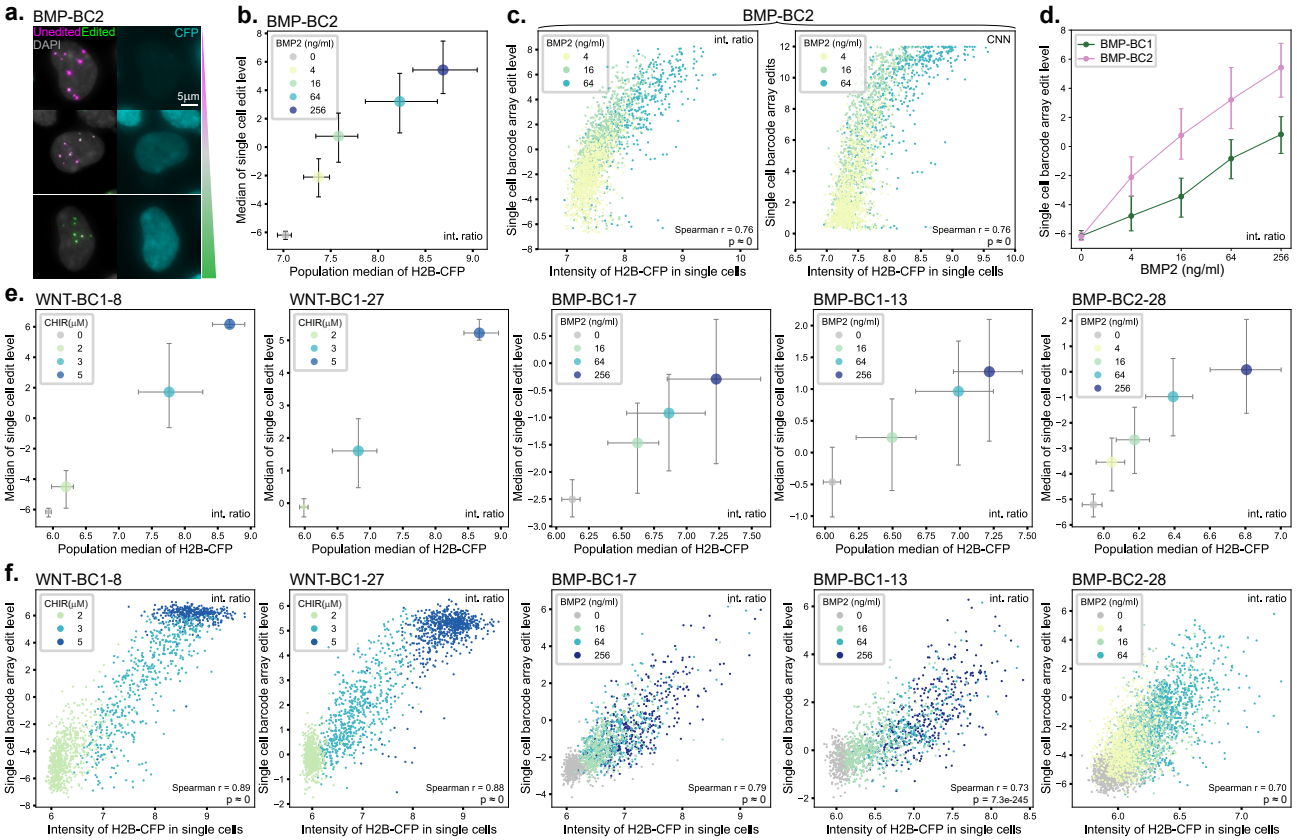

Extended Data Fig. 3 | INSCRIBE robustly recovers dose-dependent signaling across multiple independent monoclonal lines. a, Representative singel-cell images showing the editing levels and the corresponding H2B-CFP intensities in BMP-BC2. Three cells are shown with ascending response levels from top to bottom. The merged-image color bar schematically represents the edited/unedited intensity ratio. **b**, Scatter plots display median of single-cell barcode edit levels versus H2B-CFP intensity for BMP-BC2. Edit level is calculated as the average of intensity ratios across all barcode arrays in each cell. The varying levels of signal inducer, indicated by color. Bars represent the IQR. **c**, Correlation of single-cell edit levels with H2B-CFP intensities for BMP-BC2. Each point represents a single cell, colored by inducer level. Edit level in each cell is calculated either as the average of intensity ratios (left) or as the average of CNN classifier predicted edits (right) across all its barcode arrays. Spearman correlation coefficients across the inducer dosages and associated two-sided p values are shown for each plot. **d**, The median of single-cell barcode edit levels for BMP-BC1 (green) and BMP-BC2 cells (pink) across different BMP2 levels. Bars represent the IQR. **e**, Scatter plots display median of single-cell edit levels versus H2B-CFP intensities across monoclonal lines. Each subplot corresponds to an individual monoclonal. The varying levels of signal inducer, indicated by color. Bars represent the IQR. **f**, Correlation of single-cell edit levels with H2B-CFP intensities across monoclonal cell lines. Each subplot corresponds to an individual monoclonal. Each point represents a single cell, colored by inducer level. Spearman correlation coefficients across the inducer dosages and associated two-sided p values are shown for each subplot. All the recording experiments were performed over 3 days with 10 μM of TMP, using 2500 ng/ml Dox for WNT recording and 500 ng/ml Dox for BMP recording.

https://doi.org/10.1038/s41589-026-02168-3

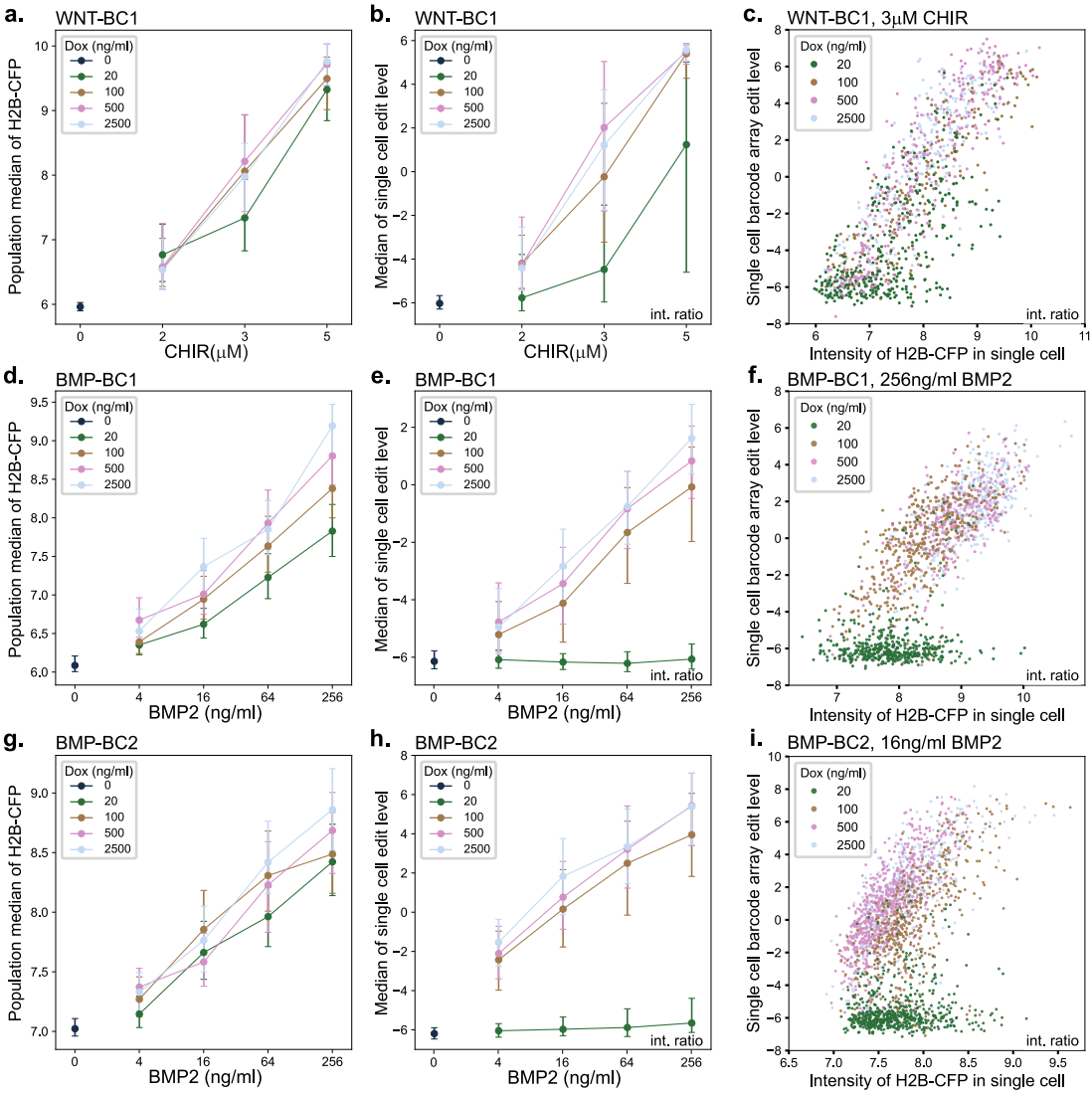

Extended Data Fig. 4 | Robustness of signal recording in the INSCRIBE cell lines with respect to the Dox concentration. a, b and **c**, Recording of the WNT pathway activity by WNT-BC1 cells. Population medians and the interquartile ranges of single cell H2B-CFP intensities (**a**), and edit levels (**b**) are plotted against CHIR concentration, with colors indicating different Dox levels. While editing requires expression of Dox inducible ABE, H2B-CFP expression is expected to be independent of Dox. The scatter plot (**c**) shows correlation between barcode edit level and H2B-CFP intensity in single cells after 3 days of recording with 3 μM CHIR. Each point in the scatter plots represents a single cell, with colors indicating the Dox concentration. Cells from recording experiments with Dox concentration ranging from 100 to 2500 ng/ml are intermixed. Similar results were obtained for BMP-BC1 cells (**d, e**, and **f**) and BMP-BC2 cells (**g, h**, and **i**). Scatter plots show the results for 3 days recording in the presence of 256 ng/ml BMP2 for BMP-BC1 cells (**f**), and 16 ng/ml BMP2 for BMP-BC2 cells (**i**). Edit level in each cell is calculated as the average of intensity ratios for all its barcode arrays.

https://doi.org/10.1038/s41589-026-02168-3

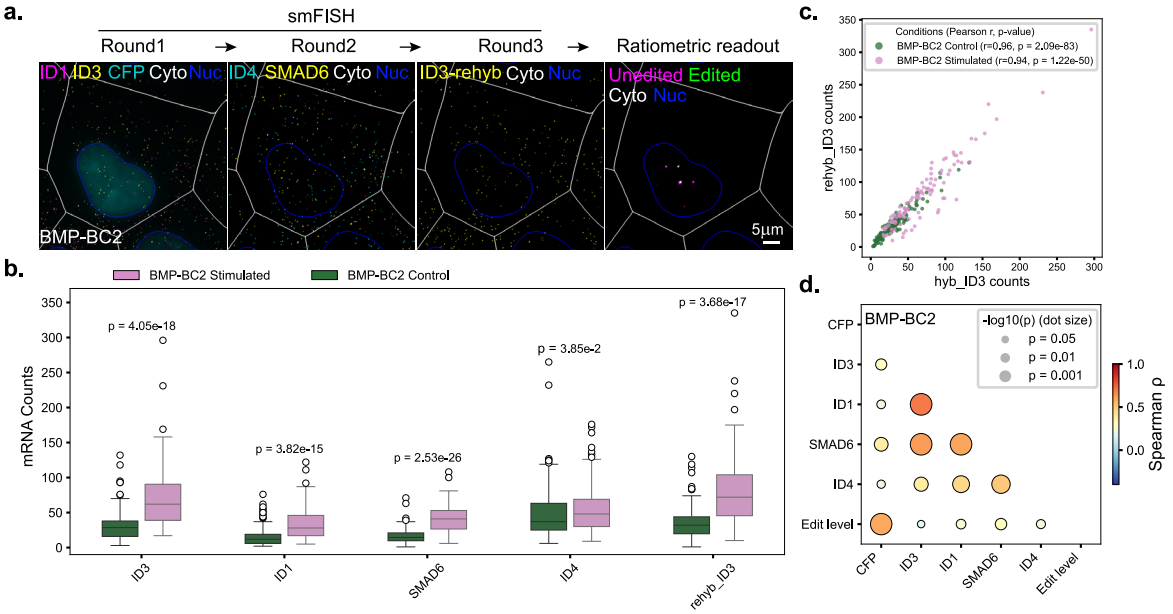

Extended Data Fig. 5 | Ratiometric barcode readout following in situ measurement of BMP target genes by multiplexed single molecule FISH. **a**, Representative images show single molecule FISH of target mRNAs, followed by ratiometric readout of barcode arrays in a BMP-BC2 cell. Cytoplasmic (Cyto) and nuclear (Nuc) boundaries are shown only as outlines for clarity. **b**, Box plot shows the single-cell mRNA counts for target mRNAs in BMP-BC2 Control (green) and BMP-BC2 Simulated (pink) cells. The boxes indicate the IQR, with center lines marking the median and whiskers extending to 1.5×IQR. Statistical significance between groups was assessed using the two-sided Mann-Whitney U test, and the corresponding p-values are shown above the box plots. **c**, Scatter plot shows the correlation of single-cell ID3 mRNA counts between initial and second hybridizations. Each point represents a single cell. Pearson correlation coefficients and associated two-sided p values are shown. **d**, Spearman correlation matrix of single cell measurements for stimulated BMP-BC2 cells. The spearman correlation coefficients are color coded, with point size proportional to the associated two-sided p values. BMP-BC2 cells stimulated with 256 ng/ml of BMP2 for 1 day.

https://doi.org/10.1038/s41589-026-02168-3

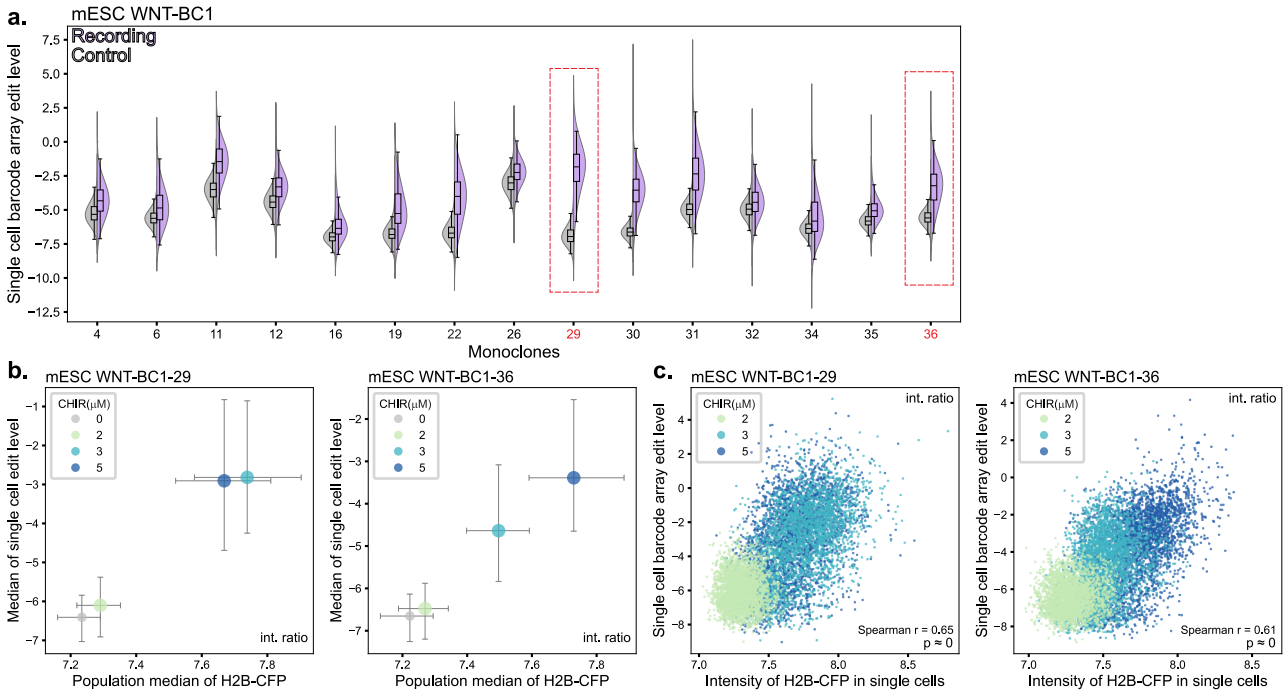

Extended Data Fig. 6 | Screening of monoclonal INSCRIBE mESC cell lines. **a**, Split violin plots show the distribution of single cell edit levels after pathway stimulation compared to the unstimulated control condition for monoclonal cell lines from mESC WNT-BC1 INSCRIBE recording configuration. The overlaid boxes indicate the IQR, with center lines marking the median and whiskers extending to 1.5×IQR. Outliers are omitted for clarity. The WNT pathway was activated by 3 μM CHIR. The lines used for further analysis are highlighted by red dotted rectangles. **b**, Scatter plots display the population median of single-cell barcode edit levels versus H2B-CFP intensity across mESC monoclonal cell lines. Each subplot corresponds to an individual monoclonal line, annotated with its INSCRIBE recording configuration and monoclonal identifier. The varying levels of signal inducer, indicated by color. Bars represent the interquartile ranges. **c**, Correlation of single-cell barcode edit levels with H2B-CFP intensities across mESC monoclonal cell lines. Each subplot corresponds to an individual monoclonal line. Each point in the scatter plots represents a single cell, with colors indicating the level of the inducer. Spearman correlation coefficients across the inducer dosages and associated two-sided *p* values are shown for each subplot. All recording experiments were performed for 3 days with 10 μM of TMP supplement, using 100 ng/ml of Dox for monoclonal screen (**a**), 500 ng/ml Dox for WNT recording (**b**-**c**). Edit level in each cell is calculated as the average of intensity ratios for all its barcode arrays.

https://doi.org/10.1038/s41589-026-02168-3

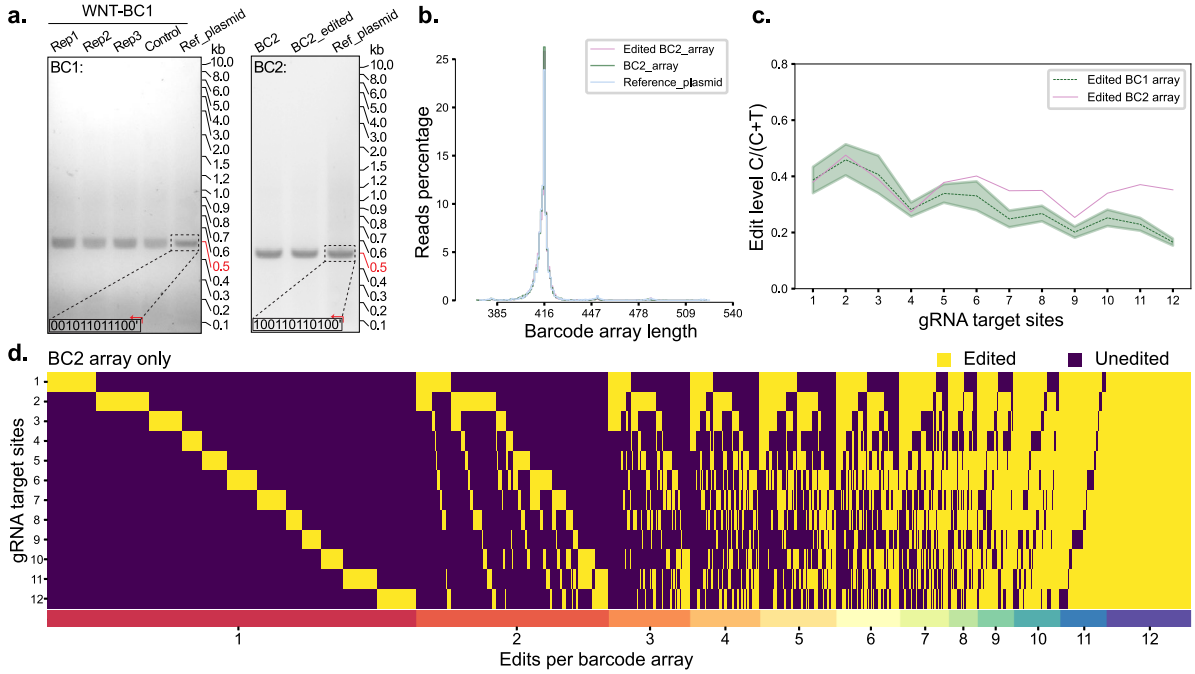

Extended Data Fig. 7 | Evaluating genomic stability and edit patterns of BC2 arrays. a, Image of DNA electrophoresis gel shows the length of amplicons from WNT-BC1 recording experiments (left, corresponding with Fig. 5b), and from transient transfection mediated BC2 array recording (right). **b**, Histogram of BC2 array lengths recovered by amplicon sequencing after transfection, compared to untransfected control populations maintained in culture for over a year. Amplified barcode array from a plasmid is included as a reference. **c**, Edit level for each gRNA target site in the BC1 (green) and BC2 array (pink) under edited conditions, corresponding with Fig. 5e. The shaded areas represent the mean ± standard deviation across three biological replicates for BC1 array. **d**, The edit status of all edited barcode arrays recovered by amplicon sequencing after 3 days of BC2 recording.

https://doi.org/10.1038/s41589-026-02168-3

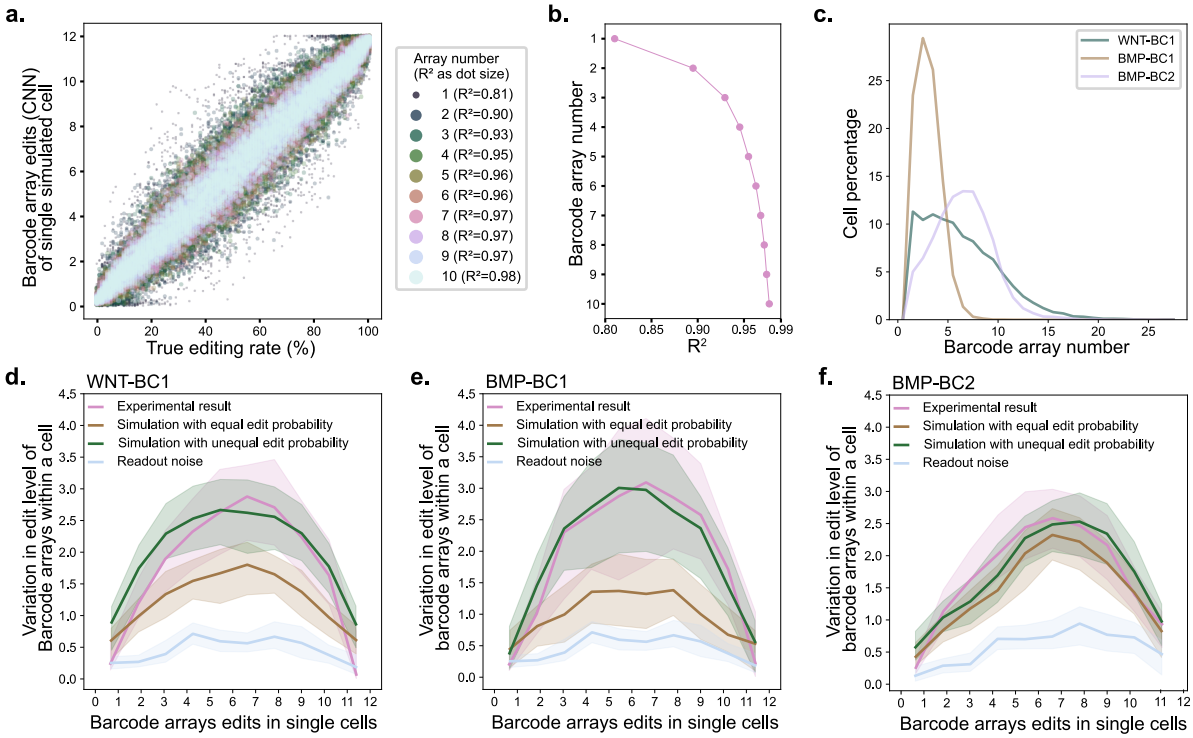

Extended Data Fig. 8 | Reconstruction accuracy and noise in signal recording by INSCRIBE. a, Scatter plot shows the single cell inferred edit level against the true edit probability for varying number of barcode arrays. Each point represents a simulated single cell, with the array number indicated by color, and the R^2 for Pearson correlation between inferred edit level and true edit probability indicated by dot size. 50 cells were simulated for each edit probability and barcode array number pair. **b**, The R^2 for Pearson correlation between inferred edit level and true edit probability across different numbers of barcode arrays per cell. **c**, Distribution of the number of barcode arrays detected in individual cells for each INSCRIBE cell line. Data from different recording durations are combined (0 to 7 days for WNT-BC1 and BMP-BC1; 0 to 6 days for BMP-BC2). WNT-BC1, BMP-BC1, and BMP-BC2 cells were stimulated by 3 μM CHIR, 256 ng/ml BMP2, and 16 ng/ml BMP2, respectively. 500 ng/ml Dox and 10 μM of TMP was used to induce ABE expression. **d-f**, The plots show population median (line) and the IQR (shaded area) for the standard deviation against the mean of edit levels of barcode arrays within a cell. Cells with arrays of known edit patterns were used to calculate the readout noise (blue). Experimental results for recording with each INSCRIBE cell line were obtained as described in Extended Data Fig. 8c (pink). Only cells with more than one array were included in the analysis. Simulations assumed either equal edit probability for all arrays within a cell (brown) or unequal probabilities generated by adding normal noise between arrays of the same cell (green). The standard deviation of normal noise was 0.21, 0.28, and 0.09 for WNT-BC1 (**d**), BMP-BC1 (**e**), and BMP-BC2 (**f**), respectively.

https://doi.org/10.1038/s41589-026-02168-3

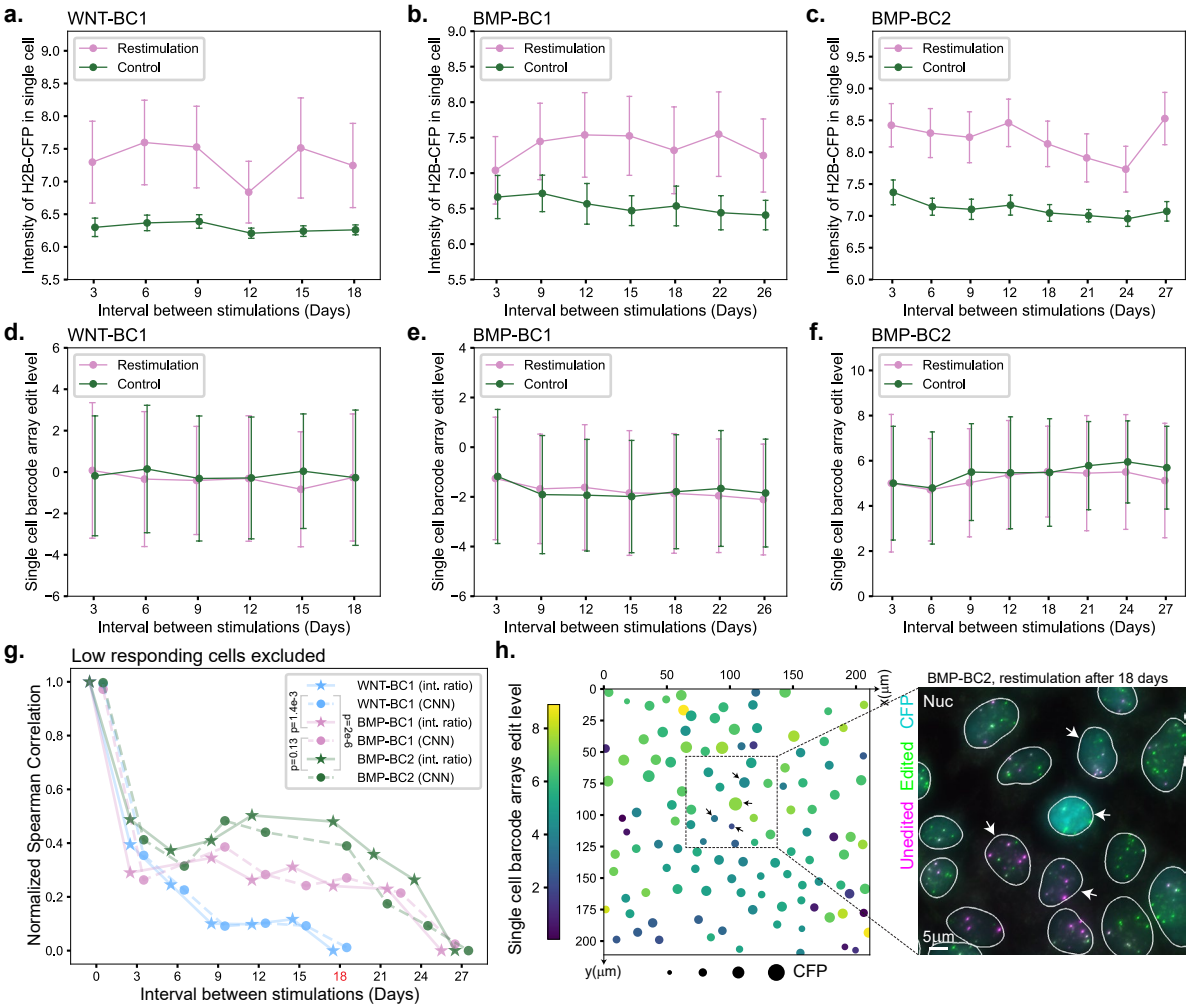

Extended Data Fig. 9 | Controls and extended analyses of WNT-BC1, BMP-BC1, and BMP-BC2 signaling memory. a-c, Population average (points) and standard deviation (bars) of single cell H2B-CFP intensity after restimulation (pink) of WNT-BC1 (**a**), BMP-BC1 (**b**) and BMP-BC2 (**c**). In the control group (green), cells were stimulated only during the first 3-day recording, and CHIR or BMP2 was omitted during the second stimulation. **d-f**, Population average (points) and standard deviation (bars) of single cell edit levels after restimulation (pink) or under control condition (green), for WNT-BC1 (**d**), BMP-BC1 (**e**) and BMP-BC2 (**f**) cells. Edit level was calculated as the average of intensity ratios for all barcode arrays in each cell. **g**, Normalized spearman correlation between the first and second response levels for the WNT-BC1 (blue), BMP-BC1(pink) and BMP-BC2 (green) across time intervals. The first response level was measured either by intensity ratio (solid line) or the CNN model (dashed line). The second response level was measured by H2B-CFP intensity. Spearman correlations were normalized to the maximum and minimum values for each line across time intervals. The cells with both the edit level, inferred by intensity ratio, and H2B-CFP intensity below the 95th percentile of unstimulated control cells are excluded. Two-sided F-tests performed on normalized Spearman correlations over time after cubic polynomial regressions, with FDR-adjusted p-values indicated. **h**, spatial context in one representative field of view for BMP-BC2 restimulated after 18 days. Each point marks a cell centroid, with size proportional to H2B-CFP intensity and color indicating edit level. A microscopy image is displayed on the right, with arrows highlighting cells exhibiting weak or strong second responses. Edit level is calculated as the average of intensity ratios across all barcode arrays in each cell. Nuclei are outlined for clarity.

nature portfolio

Corresponding author(s): Amjad Askary

Last updated by author(s): Nov 30, 2025

Reporting Summary

Nature Portfolio wishes to improve the reproducibility of the work that we publish. This form provides structure for consistency and transparency in reporting. For further information on Nature Portfolio policies, see our Editorial Policies and the Editorial Policy Checklist.

Statistics

For all statistical analyses, confirm that the following items are present in the figure legend, table legend, main text, or Methods section.

n/a	Confirmed
☐	☒ The exact sample size (*n*) for each experimental group/condition, given as a discrete number and unit of measurement
☐	☒ A statement on whether measurements were taken from distinct samples or whether the same sample was measured repeatedly
☐	☒ The statistical test(s) used AND whether they are one- or two-sided *Only common tests should be described solely by name; describe more complex techniques in the Methods section.*
☒	☐ A description of all covariates tested
☒	☐ A description of any assumptions or corrections, such as tests of normality and adjustment for multiple comparisons
☐	☒ A full description of the statistical parameters including central tendency (e.g. means) or other basic estimates (e.g. regression coefficient) AND variation (e.g. standard deviation) or associated estimates of uncertainty (e.g. confidence intervals)
☐	☒ For null hypothesis testing, the test statistic (e.g. *F*, *t*, *r*) with confidence intervals, effect sizes, degrees of freedom and *P* value noted *Give P values as exact values whenever suitable.*
☒	☐ For Bayesian analysis, information on the choice of priors and Markov chain Monte Carlo settings
☒	☐ For hierarchical and complex designs, identification of the appropriate level for tests and full reporting of outcomes
☐	☒ Estimates of effect sizes (e.g. Cohen's *d*, Pearson's *r*), indicating how they were calculated

Our web collection on statistics for biologists contains articles on many of the points above.

Software and code

Policy information about availability of computer code

Data collection	Images were collected on a Zeiss AXIO Observer Z1 inverted fluorescence microscope, using the ZEN 2.6 (blue version) for hardware control
Data analysis	Images were visualized with Fiji (Automatic updated) and ZEN 2.6 (blue version). The ratiometric FISH spots and the sequential smFISH dots were segmented with ilastik (version, 1.4.0rc2), and the cytoplasm and nuclear were segmented by cellpose 3. For experiments involving multiple rounds of imaging, images were registered using the HyperStackReg plugin in Fiji. The imaging processing and analysis pipelines were formed by either custom code using Python (3.8.16) Jupyter Notebook or custom Macro for Fiji. All Python scripts and processed source data required to replicate our analysis is provided through a Github repository (https://github.com/askarylab/INSCRIBE).

For manuscripts utilizing custom algorithms or software that are central to the research but not yet described in published literature, software must be made available to editors and reviewers. We strongly encourage code deposition in a community repository (e.g. GitHub). See the Nature Portfolio guidelines for submitting code & software for further information.

Data

Policy information about availability of data

All manuscripts must include a data availability statement. This statement should provide the following information, where applicable:

- Accession codes, unique identifiers, or web links for publicly available datasets
- A description of any restrictions on data availability
- For clinical datasets or third party data, please ensure that the statement adheres to our policy

The INSCRIBE barcode array amplicon sequencing datasets are deposited into the National Center for Biotechnology Information (NCBI)'s Sequence Read Archive, accession number PRJNA1232380. The sequence of primers, probes, and constructs used in this study are listed in Supplementary Table 1. The exact quantified sample size for each experimental condition is listed in Supplementary Table 2. All the statistical data and unprocessed gel images are included in the Source Data. The other raw data are available upon request from the corresponding author, given the large size of the imaging datasets.

Research involving human participants, their data, or biological material

Policy information about studies with human participants or human data. See also policy information about sex, gender (identity/presentation), and sexual orientation and race, ethnicity and racism.

Reporting on sex and gender	*Use the terms sex (biological attribute) and gender (shaped by social and cultural circumstances) carefully in order to avoid confusing both terms. Indicate if findings apply to only one sex or gender; describe whether sex and gender were considered in study design; whether sex and/or gender was determined based on self-reporting or assigned and methods used. Provide in the source data disaggregated sex and gender data, where this information has been collected, and if consent has been obtained for sharing of individual-level data; provide overall numbers in this Reporting Summary. Please state if this information has not been collected. Report sex- and gender-based analyses where performed, justify reasons for lack of sex- and gender-based analysis.*
Reporting on race, ethnicity, or other socially relevant groupings	*Please specify the socially constructed or socially relevant categorization variable(s) used in your manuscript and explain why they were used. Please note that such variables should not be used as proxies for other socially constructed/relevant variables (for example, race or ethnicity should not be used as a proxy for socioeconomic status). Provide clear definitions of the relevant terms used, how they were provided (by the participants/respondents, the researchers, or third parties), and the method(s) used to classify people into the different categories (e.g. self-report, census or administrative data, social media data, etc.) Please provide details about how you controlled for confounding variables in your analyses.*
Population characteristics	*Describe the covariate-relevant population characteristics of the human research participants (e.g. age, genotypic information, past and current diagnosis and treatment categories). If you filled out the behavioural & social sciences study design questions and have nothing to add here, write "See above."*
Recruitment	*Describe how participants were recruited. Outline any potential self-selection bias or other biases that may be present and how these are likely to impact results.*
Ethics oversight	*Identify the organization(s) that approved the study protocol.*

Note that full information on the approval of the study protocol must also be provided in the manuscript.

Field-specific reporting

Please select the one below that is the best fit for your research. If you are not sure, read the appropriate sections before making your selection.

☒ Life sciences ☐ Behavioural & social sciences ☐ Ecological, evolutionary & environmental sciences

For a reference copy of the document with all sections, see nature.com/documents/nr-reporting-summary-flat.pdf

Life sciences study design

All studies must disclose on these points even when the disclosure is negative.

Sample size	No statistical methods were used to predetermine sample sizes. 7 to 9 fields of view were imaged in each condition for the same experiment to ensure sufficient representation of variability in the results.
Data exclusions	No data were excluded for the analyses, except for the cells in the boundary of filed of view which were not completely imaged.
Replication	Biological replicates correspond to multiple monoclonal cell lines subjected to the same experimental pipeline, and all attempts at replication were successful.
Randomization	We imaged cells from randomly-chosen and same number of fields of view for each conditions in the same experiment. And all the cells in the imaged fields of views were analysis through the imaging processing pipelines.

Blinding	Investigators were not blinded to group allocation. However, for all quantitative results, fields of view during imaging were chosen solely based on DAPI signal to avoid bias.

Reporting for specific materials, systems and methods

We require information from authors about some types of materials, experimental systems and methods used in many studies. Here, indicate whether each material, system or method listed is relevant to your study. If you are not sure if a list item applies to your research, read the appropriate section before selecting a response.

Materials & experimental systems

n/a	Involved in the study
☒	☐ Antibodies
☐	☒ Eukaryotic cell lines
☒	☐ Palaeontology and archaeology
☒	☐ Animals and other organisms
☒	☐ Clinical data
☒	☐ Dual use research of concern
☒	☐ Plants

Methods

n/a	Involved in the study
☒	☐ ChIP-seq
☒	☐ Flow cytometry
☒	☐ MRI-based neuroimaging

Eukaryotic cell lines

Policy information about cell lines and Sex and Gender in Research

Cell line source(s)	HEK293 (ATCC), mESCs (female, pSM44)
Authentication	Cell lines were not authenticated
Mycoplasma contamination	HEK293 cell line were certified as mycoplasma free when purchased from ATCC, no further mycoplasma contamination tested. Mycoplasma screening was performed for mESCs every two weeks.
Commonly misidentified lines (See ICLAC register)	No commonly misidentified cell lines were used in this study.

Plants

Seed stocks	*Report on the source of all seed stocks or other plant material used. If applicable, state the seed stock centre and catalogue number. If plant specimens were collected from the field, describe the collection location, date and sampling procedures.*
Novel plant genotypes	*Describe the methods by which all novel plant genotypes were produced. This includes those generated by transgenic approaches, gene editing, chemical/radiation-based mutagenesis and hybridization. For transgenic lines, describe the transformation method, the number of independent lines analyzed and the generation upon which experiments were performed. For gene-edited lines, describe the editor used, the endogenous sequence targeted for editing, the targeting guide RNA sequence (if applicable) and how the editor was applied.*
Authentication	*Describe any authentication procedures for each seed stock used or novel genotype generated. Describe any experiments used to assess the effect of a mutation and, where applicable, how potential secondary effects (e.g. second site T-DNA insertions, mosiacism, off-target gene editing) were examined.*